

Extension of the measurement of the dijet mass cross section at high rapidity

Pavel Demine, Christophe Royon, ????

July 31, 2003

Abstract

We present a detailed description of the inclusive dijet mass cross section measurement within $|\eta| < 2.4$ using 92.4 pb^{-1} of Run II data. All jets are reconstructed using the cone algorithm with a radius of 0.7.

1 Event and run selection

1.1 Data sample

The data used in this analysis were taken between September 3, 2002 and June 19, 2003. During this time period four major versions of the trigger list were used, trigger list versions 8, 9, 10 and 11. There were no major changes in jet triggers between the three versions that would affect the measurement. The measurement is done using Jet Energy Scale (JES) corrections of version 4.1.

1.2 Run selection

The data used for the present were reconstructed with versions p13.05 and p13.06 of the DØ software.

For the present analysis all the runs known to have problems with tracking and/or calorimetry were removed. The following sources of information were used:

- DØ Offline Run Quality Database:

- SMT bad runs;
- CFT bad runs;
- Calorimeter bad runs;
- Jet/MET bad runs.

run numbers	reco version
151 817 — 164 381	p13.06.01
164 382 — 168 516	p13.05.00
165 589 — 166 339	r13.06.01
168 522 — 168 571	r13.06.01
168 587 — 169 002	r13.06.01
169 171 — 169 315	p13.05.00
169 521 — 170 043	p13.06.01
170 238 — 170 246	p13.05.00
170 247 — 170 374	p13.06.01
175 757 — 178 310	p13.06.01

Table 1: Runs and d0reco versions used for the dijet analysis.

The Jet/MET selection is based on the uniformity of the ME_T and SE_T spectra [?].

Also the data taken between February 10, 2003 and April 14, 2003 are known to have so called *shared energy problem*. And all runs corresponding to this period were removed from the analysed sample.

Figures 1 and 2 represent the average number of good and bad jets per run. A good jet is defined as a jet with $E > 40$ GeV which passes all jet id cuts. The number of selected events after all cuts is shown in Figure 3. We see some differences due to the change in trigger list versions.

Trig. list ver.	Comments
8.20 — 8.41	JT_25TT_NG is added, $-0.2 < \text{EMF} < 1.2$
9.20	
9.30	JT_65TT and JT_95TT get L2 (3×3)
9.31 — 9.50	L2 jet $3 \times 3 \rightarrow 5 \times 5$
10.00	
10.01	L1 eta $2.4 \rightarrow 3.2$
10.02	L1 eta $3.2 \rightarrow 2.4$
10.03 — 10.36	L1 eta $3.2 \rightarrow 2.4$ properly
11.00 — 11.04	L1 eta $2.4 \rightarrow 3.2$

Table 2: Changes in the trigger list concerning the dijet analysis.

To understand how the changes in trigger lists affect the analysis, data taken with different trigger list versions were analysed separately. Table 2 summarizes the changes in the trigger list that could concern the dijet analysis. Based on this information, the analysed data were divided in the following subsamples:

- v8_a (8.20 — 8.41)

- v9_a (9.20)
- v9_b (9.30)
- v9_c (9.31 — 9.50)
- v10_a (10.00, 10.03 — 10.36)
- v11_a (11.00 — 11.04)

These trigger list versions cover the runs between 162 458 and 178 310

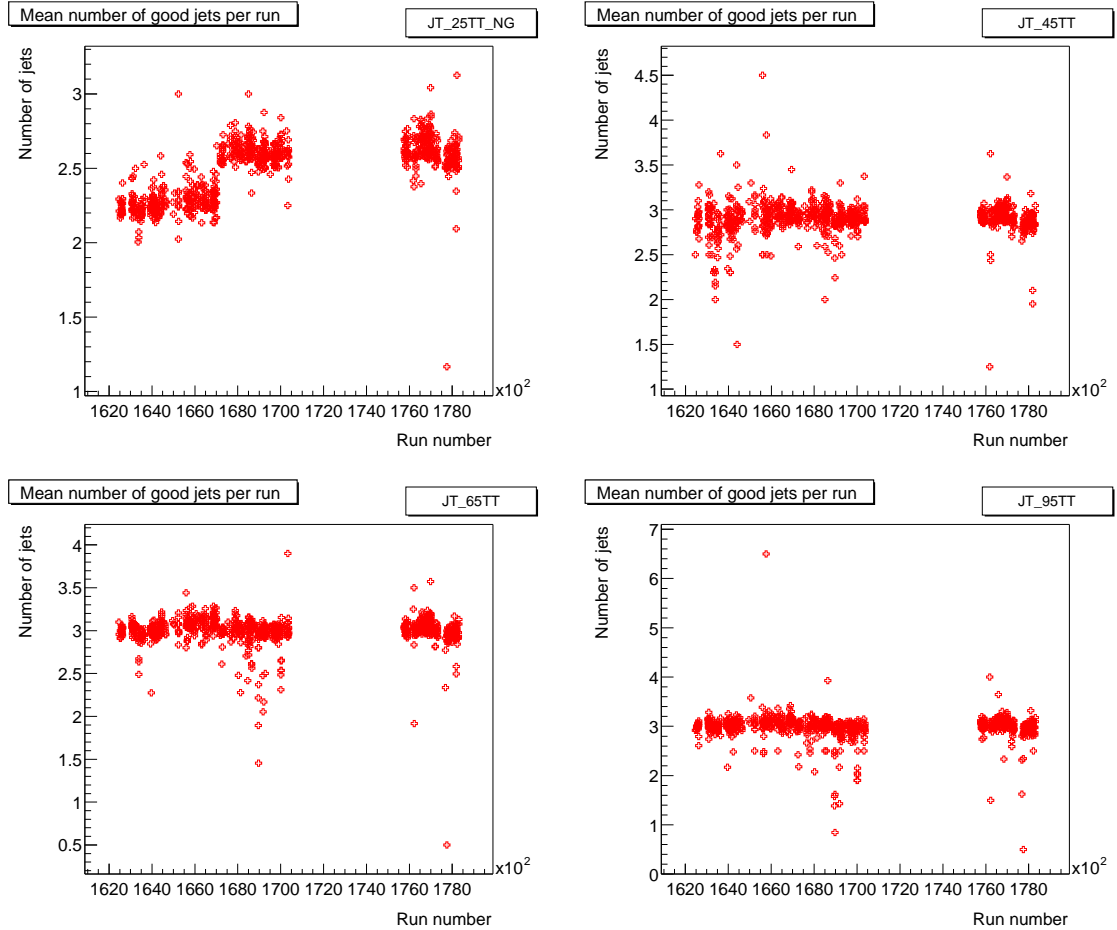


Figure 1: Mean number of good jets with $E > 40$ GeV per run for the JT_25TT_NG, JT_45TT, JT_65TT and JT_95TT triggers.

2 Event selection

In this section, we discuss the event and jet cuts used in the analysis. We show plots of the different cuts in the different bins in η_{max} and triggers used in the analysis (η_{max} is

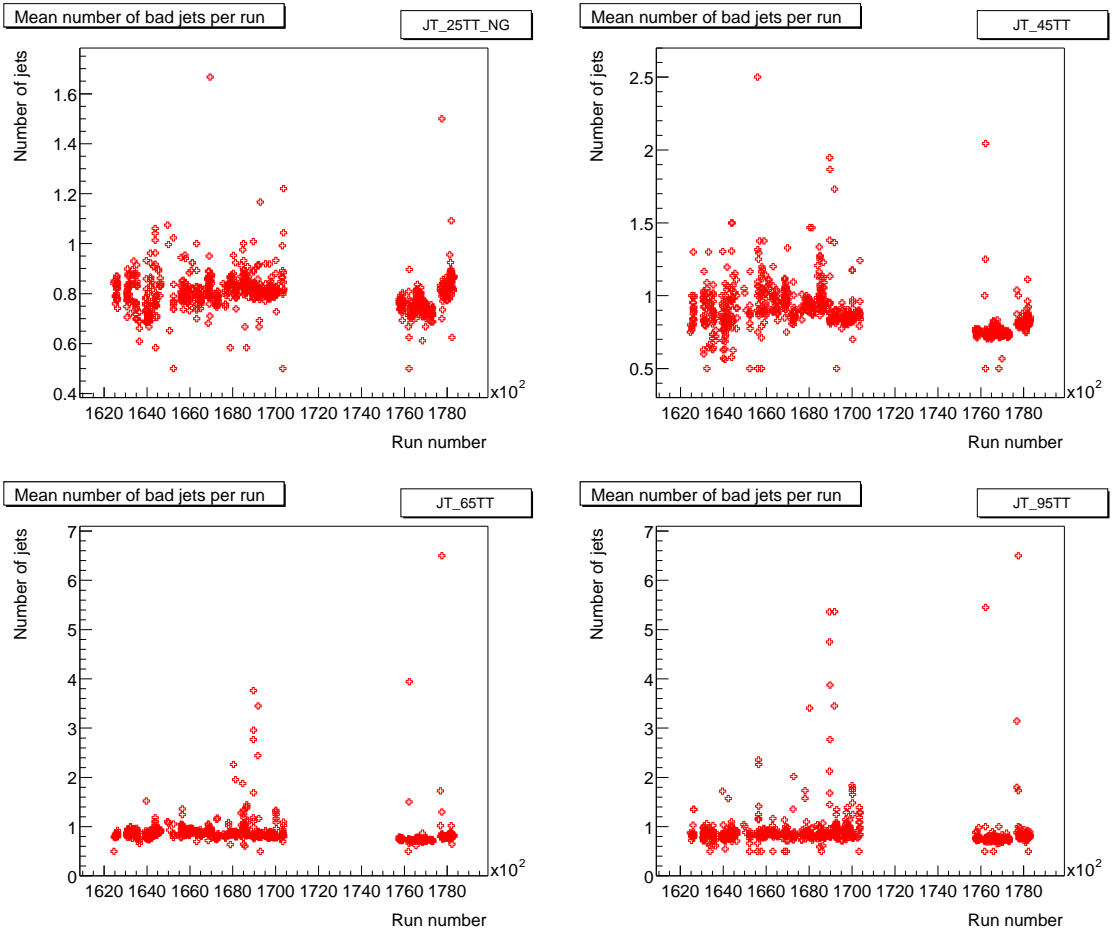


Figure 2: Mean number of bad jets with $E > 40$ GeV per run for the JT_25TT_NG, JT_45TT, JT_65TT and JT_95TT triggers.

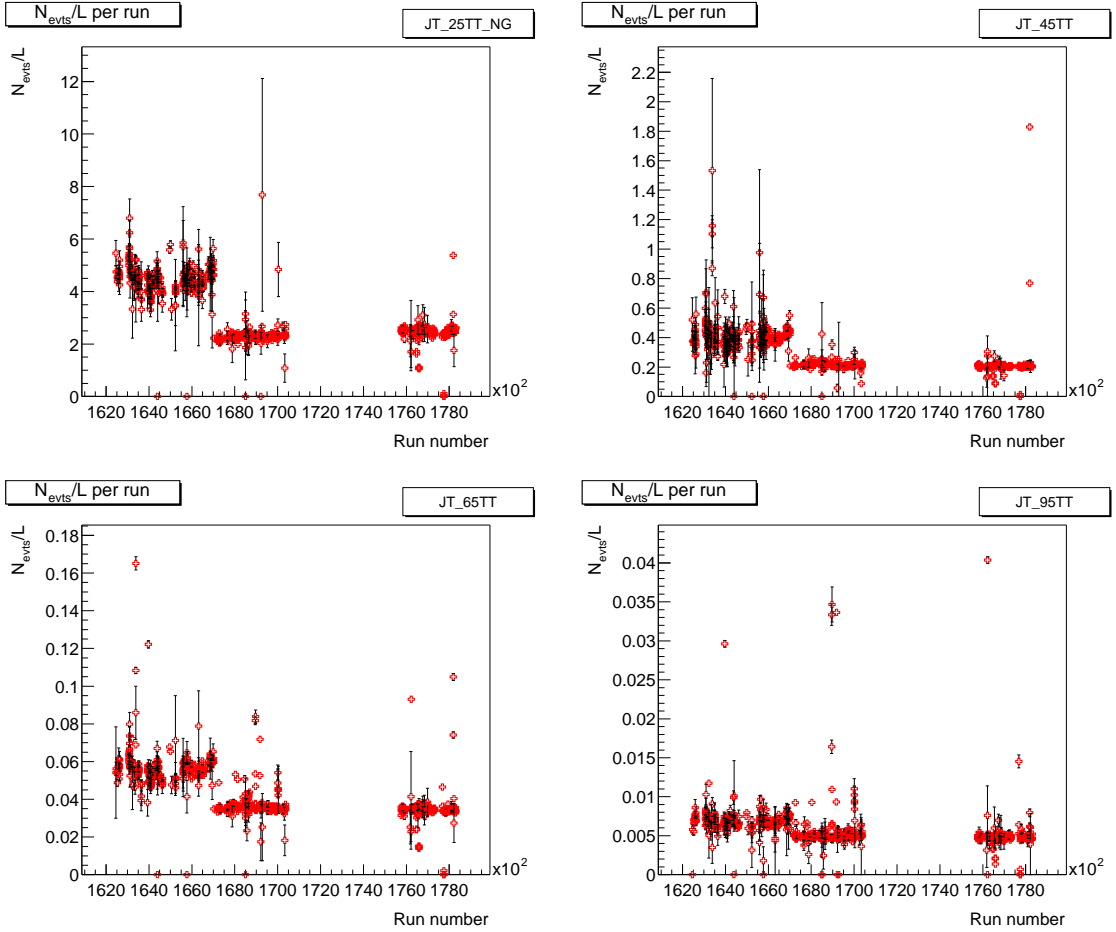


Figure 3: Number of selected events per run after all cuts, without any efficiency or unsmeared corrections for the JT_25TT_NG, JT_45TT, JT_65TT and JT_95TT triggers. We see differences due to the different trigger versions.

the maximum η of the two jets).

2.1 Trigger selection

All events in this analysis are requested to fulfil the jet trigger requirements. We select events passing the JT_25TT_NG, JT_45TT, JT_65TT and JT_95TT jet triggers. The total integrated luminosity for each trigger (after good runs and trigger list versions selection) is $\mathcal{L}_{25} = 0.64 \text{ pb}^{-1}$, $\mathcal{L}_{45} = 14.2 \text{ pb}^{-1}$, $\mathcal{L}_{65} = 61.3 \text{ pb}^{-1}$, and $\mathcal{L}_{95} = 92.4 \text{ pb}^{-1}$.

We assume that each of the four jet triggers becomes fully efficient for events with a leading jet of sufficient transverse momentum. To find out where these triggers become efficient, we plot the ratio of the uncorrected leading jet cross sections as a function of leading jet p_T for each trigger over the next lower trigger. If the cross sections are the same, then the higher trigger is as efficient as the lower trigger. We assume this efficiency is 100 %. The resulting turn on curves for different bins in detector η_{det} and different trigger list versions are shown in Figures 4–21. Only jets from the events which pass all cuts described in the section 2.3 contribute to the shown turn on curves. The values of the turn on points are given in Table 3.

Trigger	JT_25TT_NG	JT_45TT	JT_65TT	JT_95TT
leading jet p_T^{\min} , GeV/c	60.0	80.0	100.0	140.0

Table 3: Leading jet p_T turn on values for different jet triggers.

2.2 Jet cuts

The jet cuts used in the analysis are the usual cuts defined by the Jet and MET identification group, namely:

- $CHF < 0.4$
- $0.05 < EMF < 0.95$
- $hotF < 10$
- $n90 > 1$
- either $CHF < 0.15$ or $f90 < 0.5$

2.3 Event cuts

The event cuts are the following:

- Primary vertex, with at least 5 tracks fitted to it and with $|z_{vertex}| < 50 \text{ cm}$;
- $METC/p_T < 0.7$, where p_T is the corrected transverse momentum of the leading jet in the event;

- $METC < 199.9$ because of a bug on METC precision in the thumbnails.
- At least two jets are required to pass the jet cuts.
- Leading jet is in a p_T range corresponding to one of the fired jet triggers.

Figures ??–?? show three different distributions of the primary vertex position z , namely the distribution of all events (putting at $z = 0$ the events without vertex), of events having a vertex with at least 5 tracks fitted to it, and of events with additionally $|z_{vtx}| < 50$ cm. The number of tracks fitted to the vertex with the same conditions are shown in Figures ??–??. All the distributions are presented in different η_{max} and for different jet triggers. We clearly see, as expected, that the events with a $z_{vtx} > 50$ cm show less tracks fitted to them since they are more forward. We also notice that the proportion of events showing less than 5 tracks fitted to the vertex is smaller at medium rapidity.

The distributions of $p_T/METC$ in the same bins are shown in Figures ??–??. This cut was used in Run I inclusive jet p_T and dijet mass analysis to remove the cosmic, single jet like, events. We do not see many events of this kind in our sample since we already select events with at least two good jet. In the ICD region, a few events show a low value of p_T/MET , but this is still less than ???% of the total sample.

2.4 Kinematic distributions after all cuts

In this section, we give the kinematic distributions of all events after all cuts in the different trigger and η_{max} bins. We give the φ , η , and $\Delta\varphi$ distributions between jets. We also give the p_T distributions for the leading and second leading jet for different triggers and in different η_{max} bins.

3 Uncorrected cross section determination

We aim to measure the dijet mass cross section in different bins of η_{max} where η_{max} is the maximum η of the two jets.

The differential dijet mass cross section in each η_{max} bin averaged over the mass bin is computed using the following formula

$$\left\langle \frac{d\sigma}{dM_{JJ}} \right\rangle = \frac{N_{evt}}{L} \cdot \frac{1}{\Delta M_{JJ}} \quad (1)$$

where N_{evt} , L , ΔM_{JJ} are the number of events, the luminosity, and the dijet mass bin width respectively.

The uncorrected dijet cross section as function of dijet mass for the different trigger list versions and different η_{max} bins are shown in Figures 22–??. And finally, the uncorrected dijet cross section for the complete data sample is shown in Figure 27.

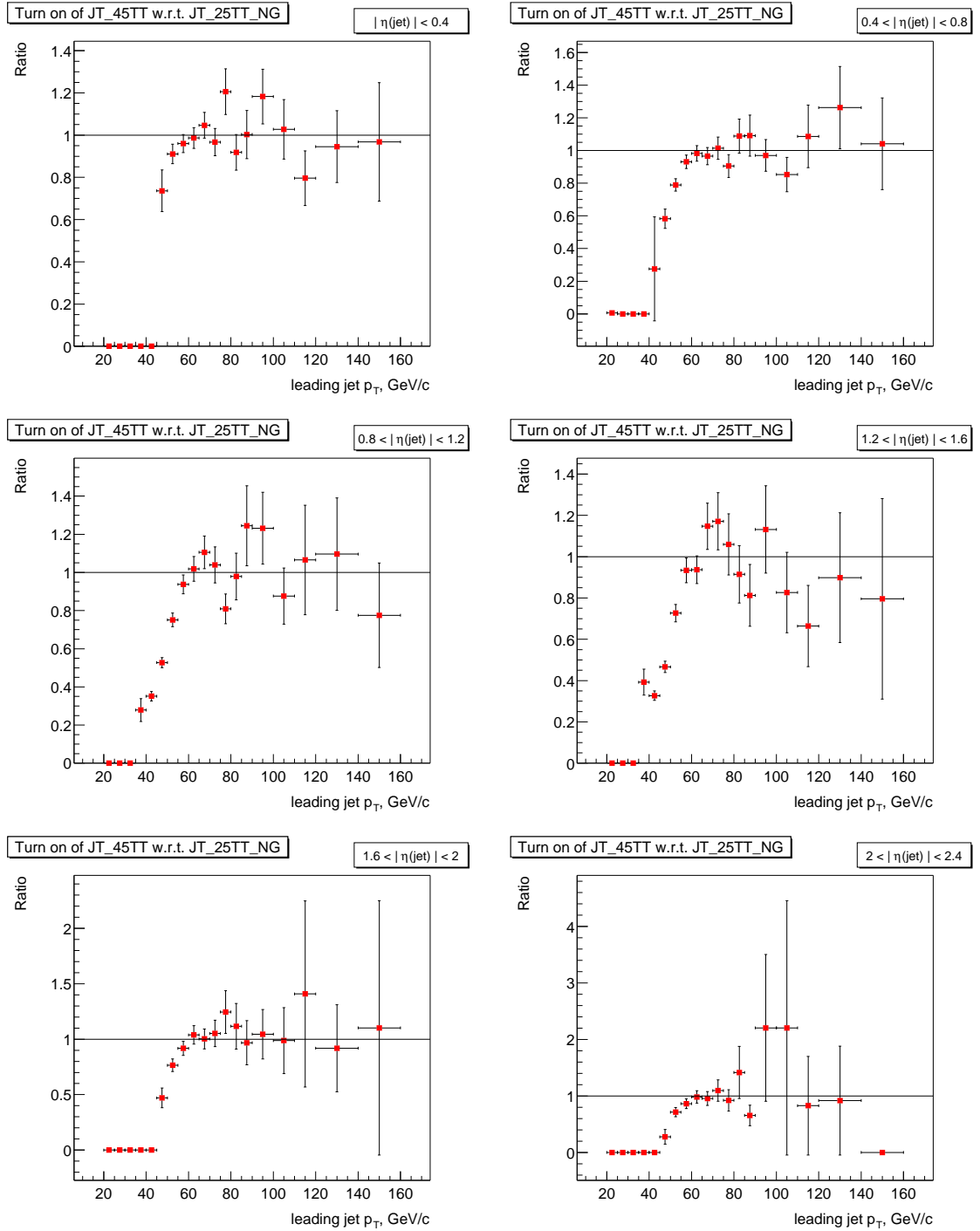


Figure 4: Turn on curves in the different η_{det} bins for JT_45TT trigger with respect to the JT_25TT_NG trigger. For trigger lists v8.20 — v8.41.

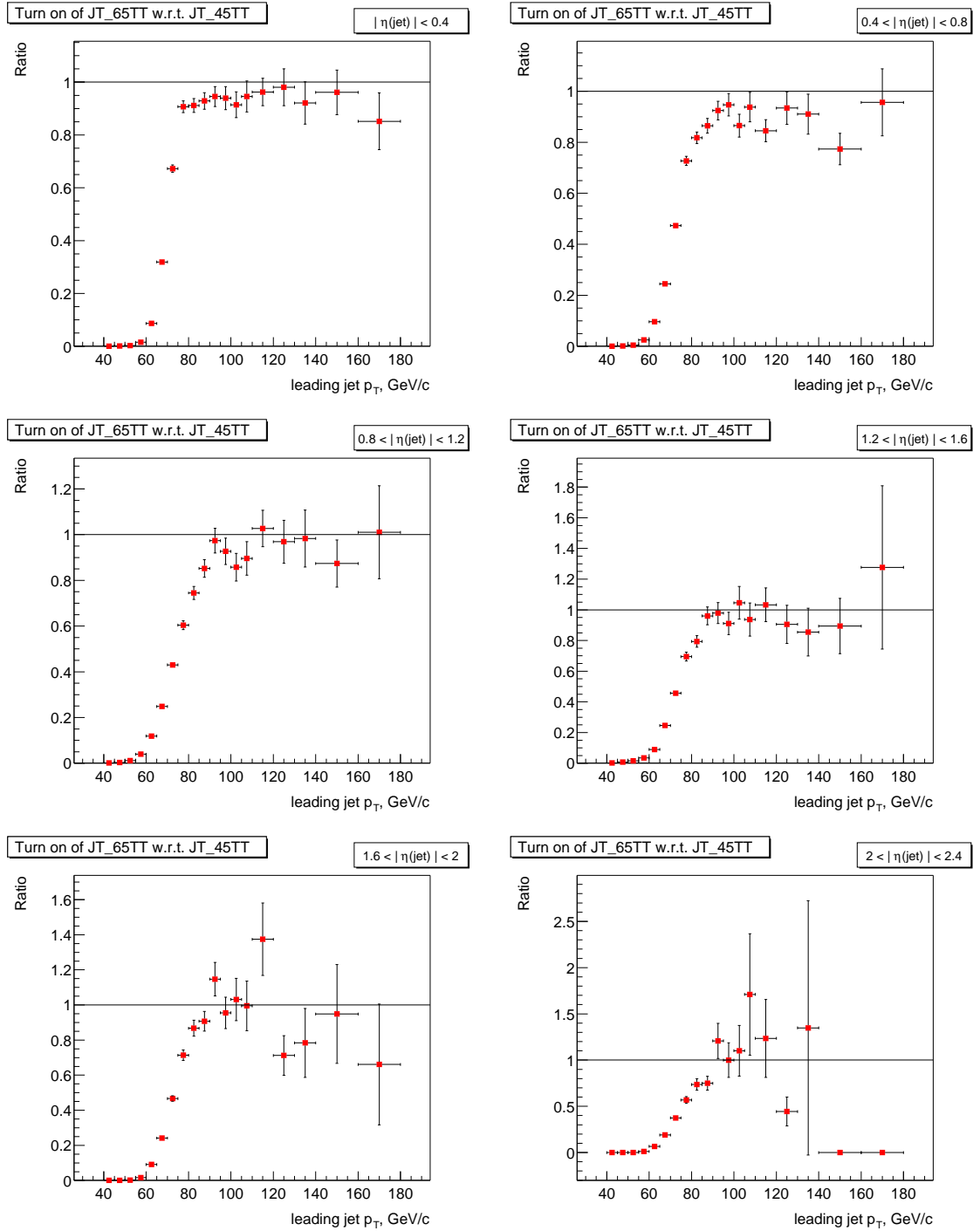


Figure 5: Turn on curves in the different η_{det} bins for JT_65TT trigger with respect to the JT_45TT trigger. For trigger lists v8.20 — v8.41.

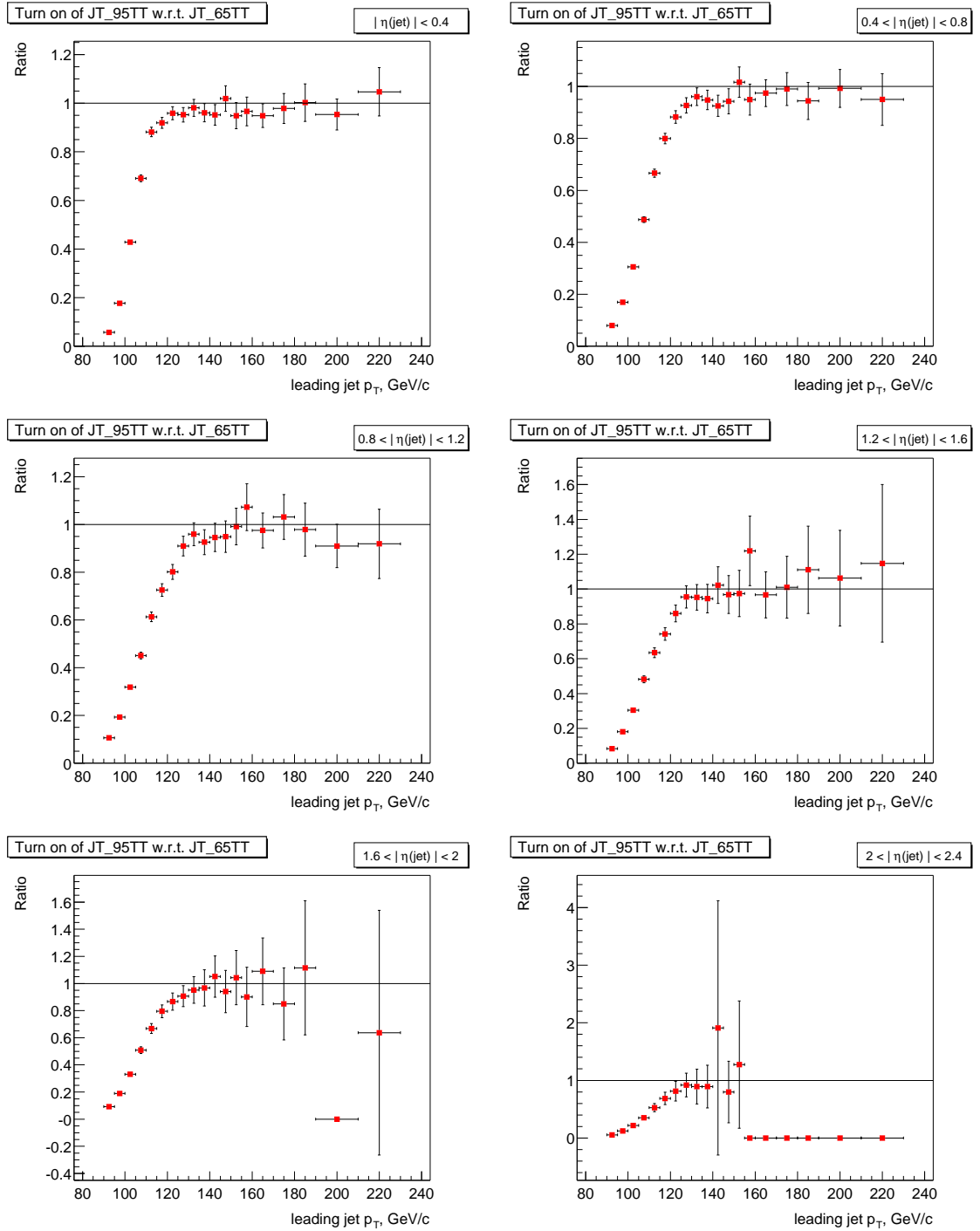


Figure 6: Turn on curves in the different η_{det} bins for JT_95TT trigger with respect to the JT_65TT trigger. For trigger lists v8.20 — v8.41.

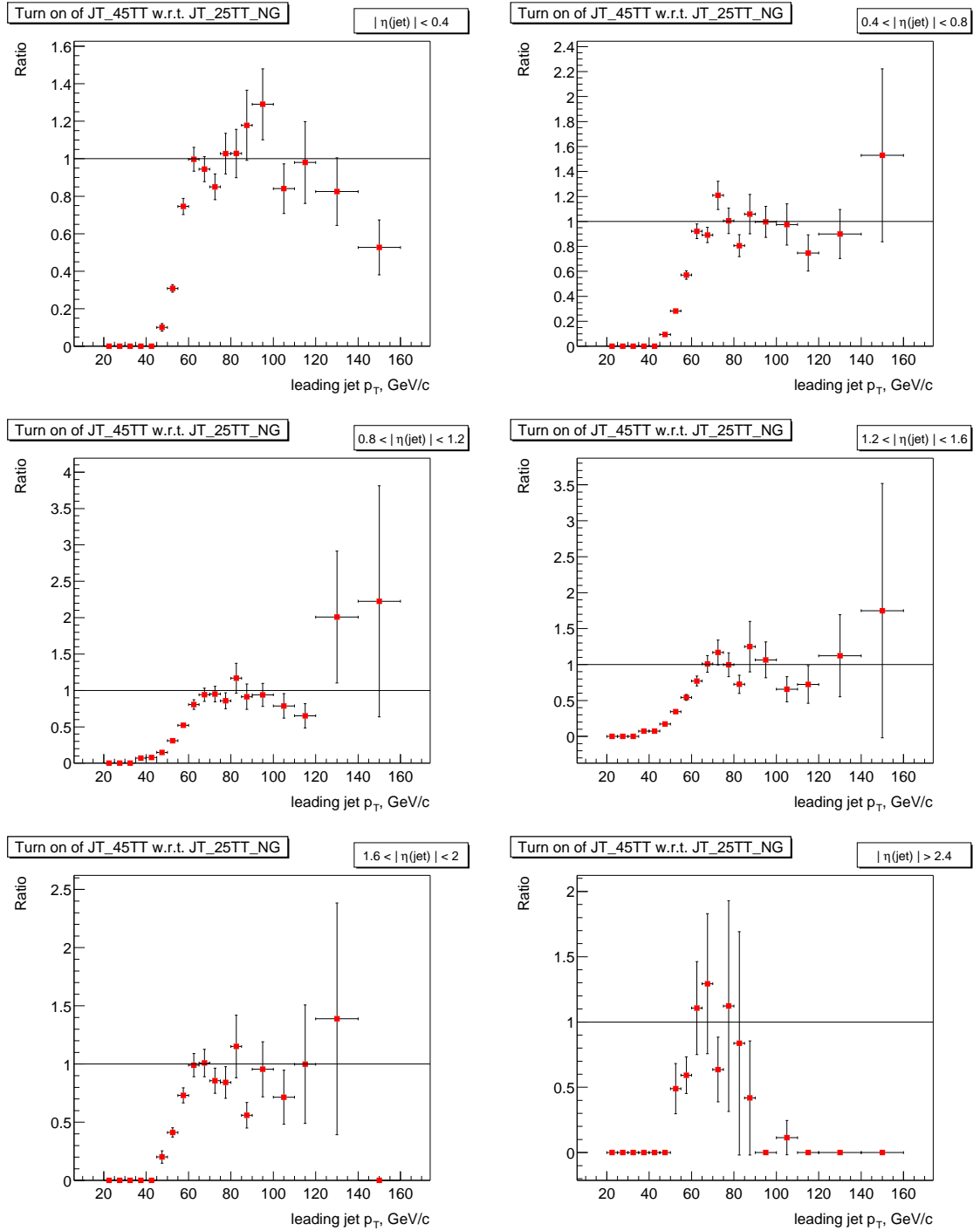


Figure 7: Turn on curves in the different η_{det} bins for JT_45TT trigger with respect to the JT_25TT_NG trigger. For trigger list v9.20.

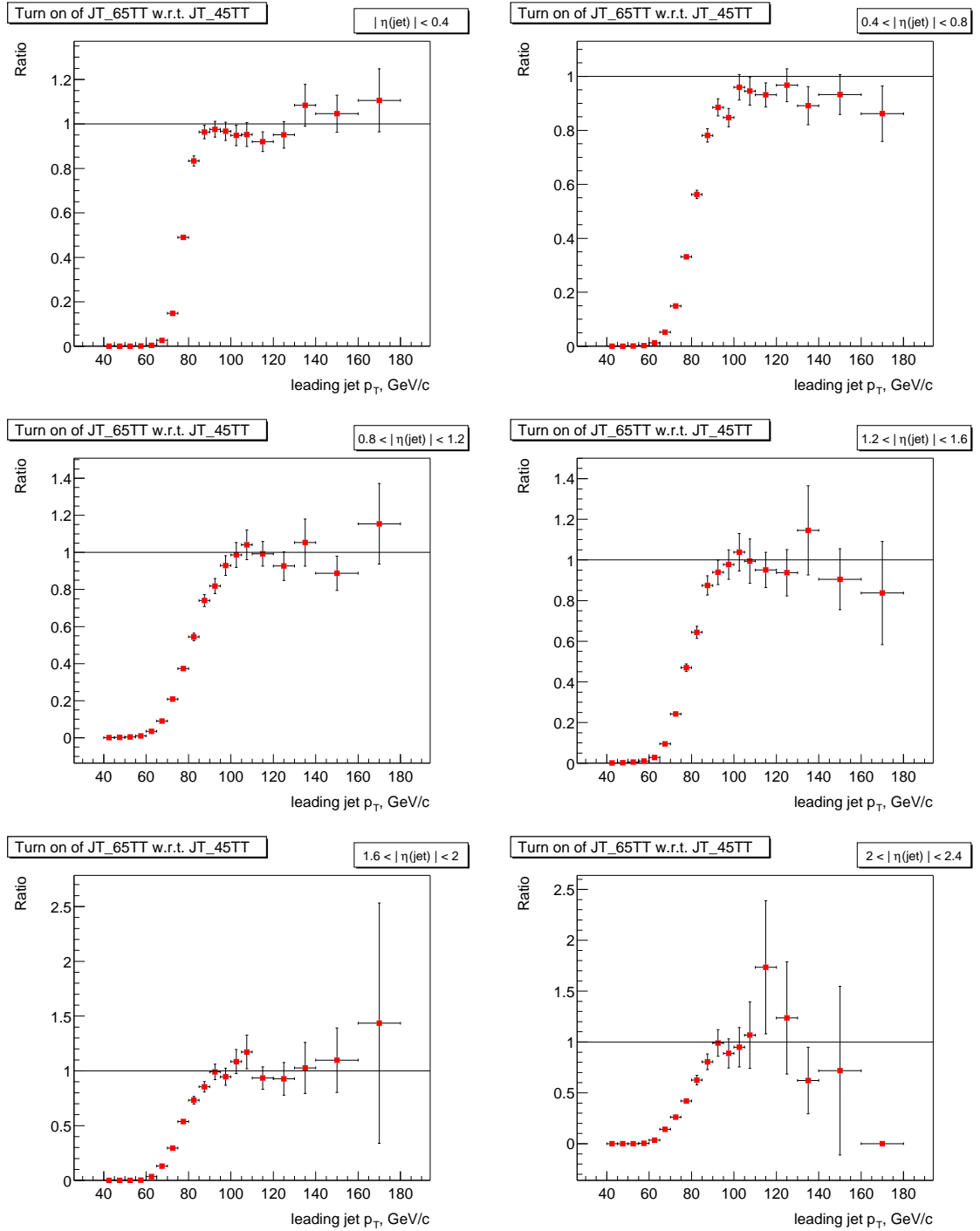


Figure 8: Turn on curves in the different η_{det} bins for JT_65TT trigger with respect to the JT_45TT trigger. For trigger list v9.20.

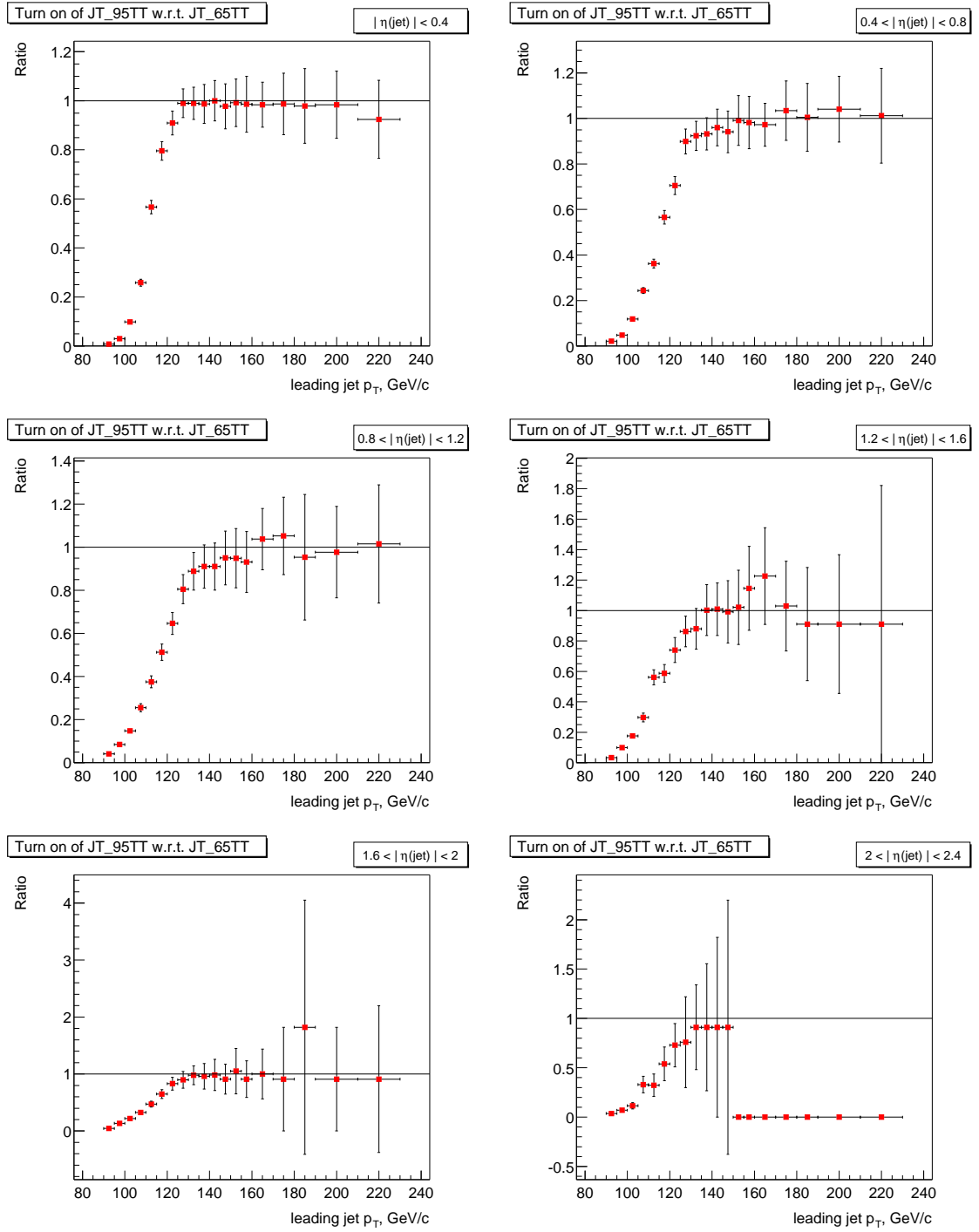


Figure 9: Turn on curves in the different η_{det} bins for JT_95TT trigger with respect to the JT_65TT trigger. For trigger list v9.20.

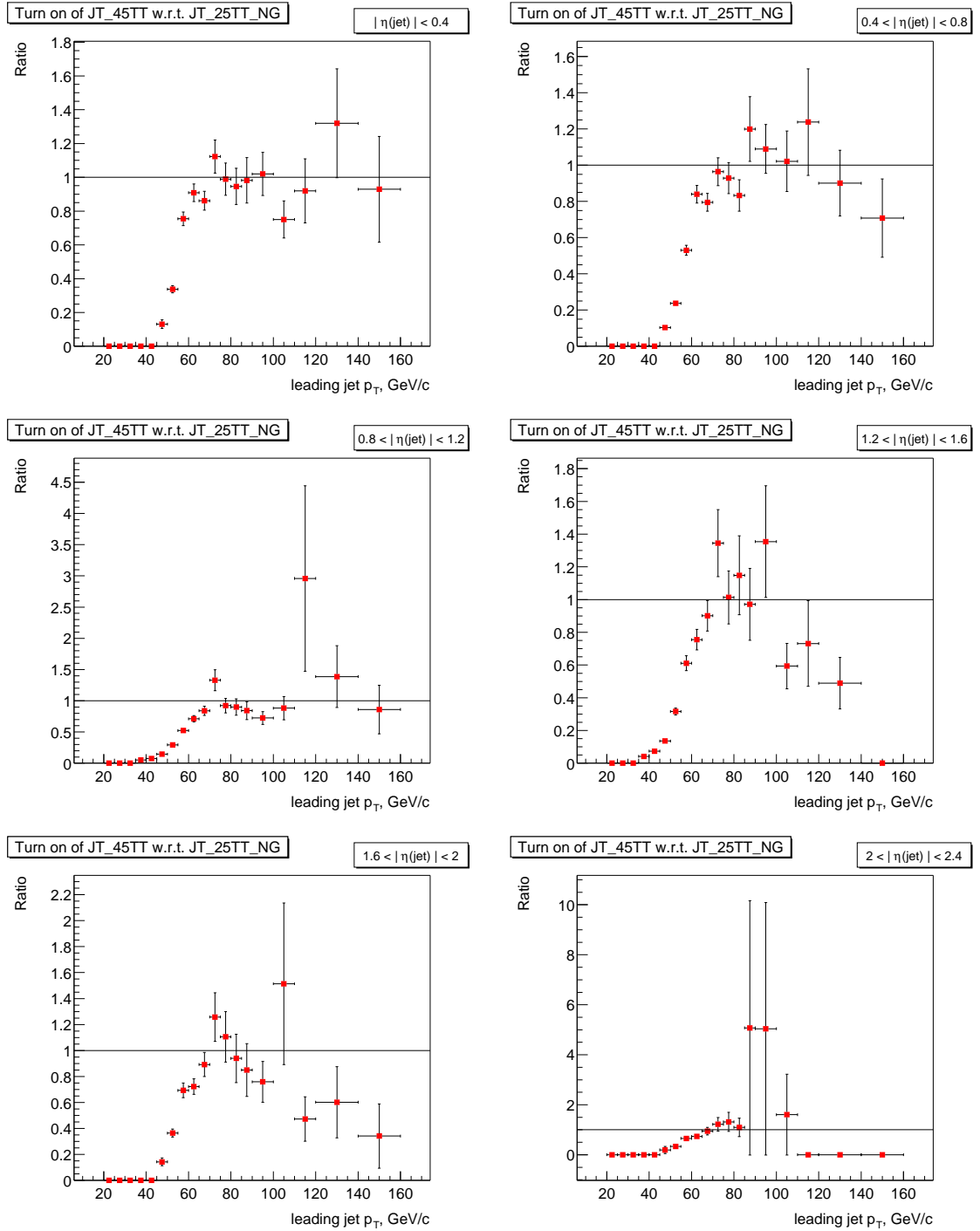


Figure 10: Turn on curves in the different η_{det} bins for JT_45TT trigger with respect to the JT_25TT_NG trigger. For trigger list v9.30.

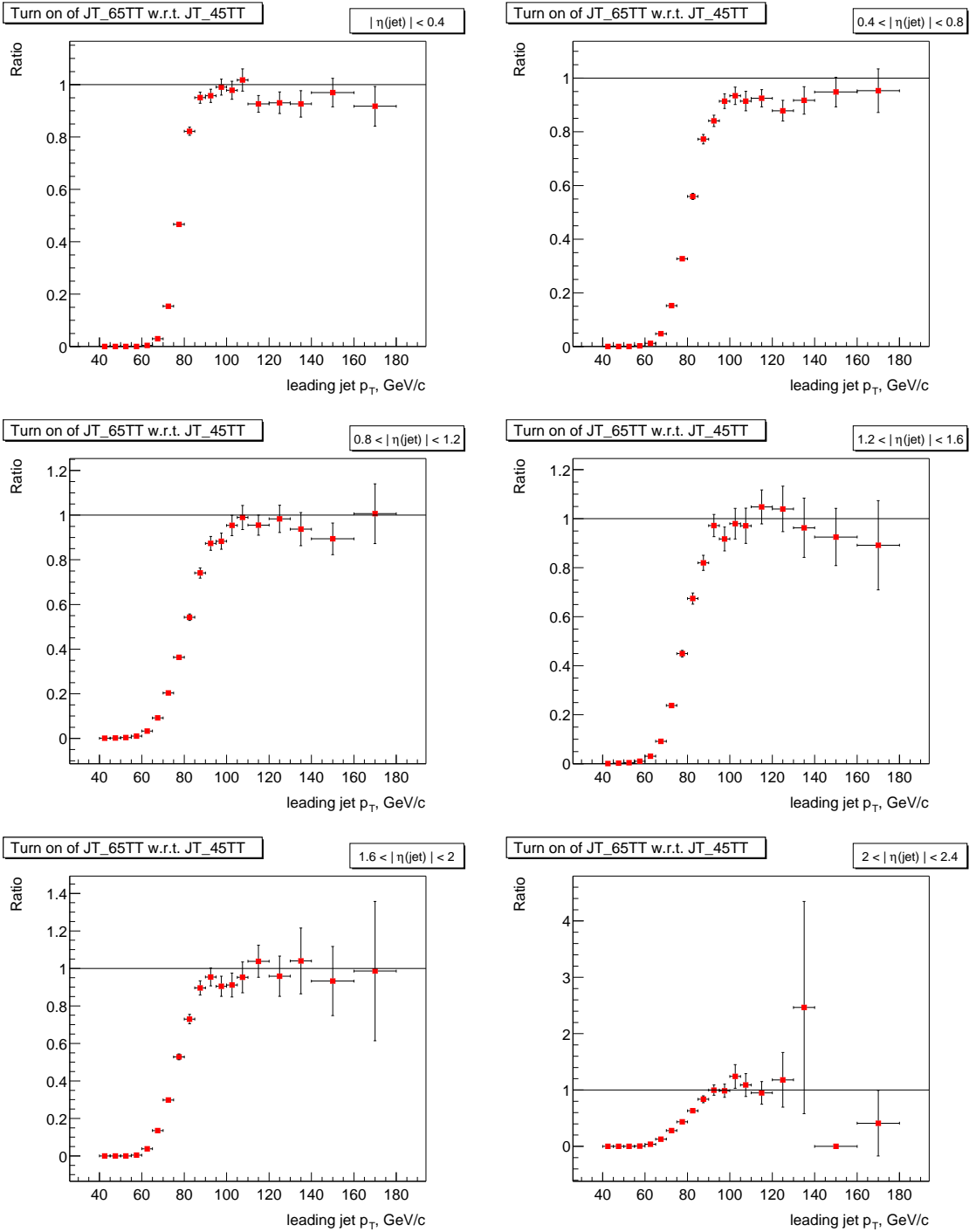


Figure 11: Turn on curves in the different η_{det} bins for JT_65TT trigger with respect to the JT_45TT trigger. For trigger list v9.30.

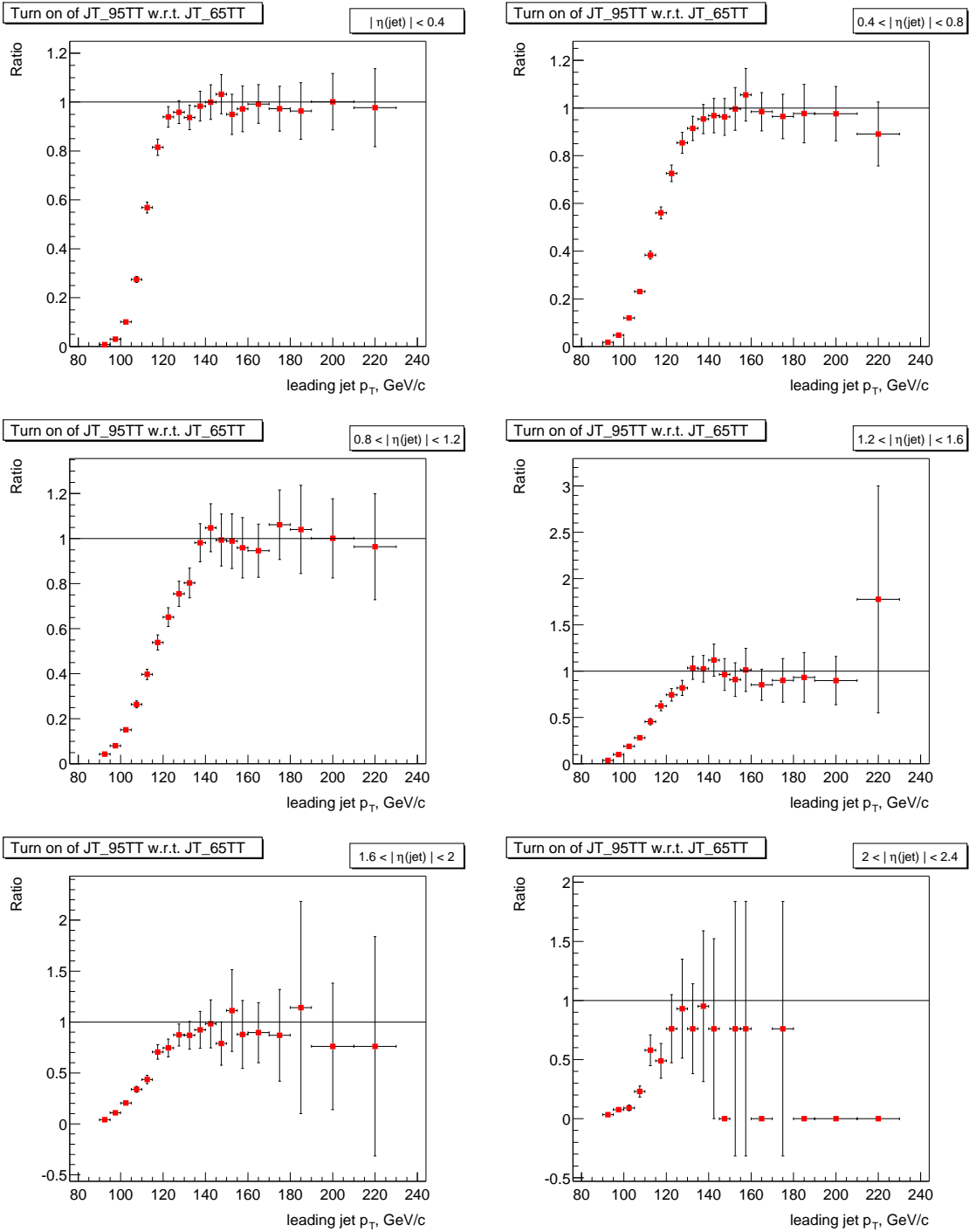


Figure 12: Turn on curves in the different η_{det} bins for JT_95TT trigger with respect to the JT_65TT trigger. For trigger list v9.30.

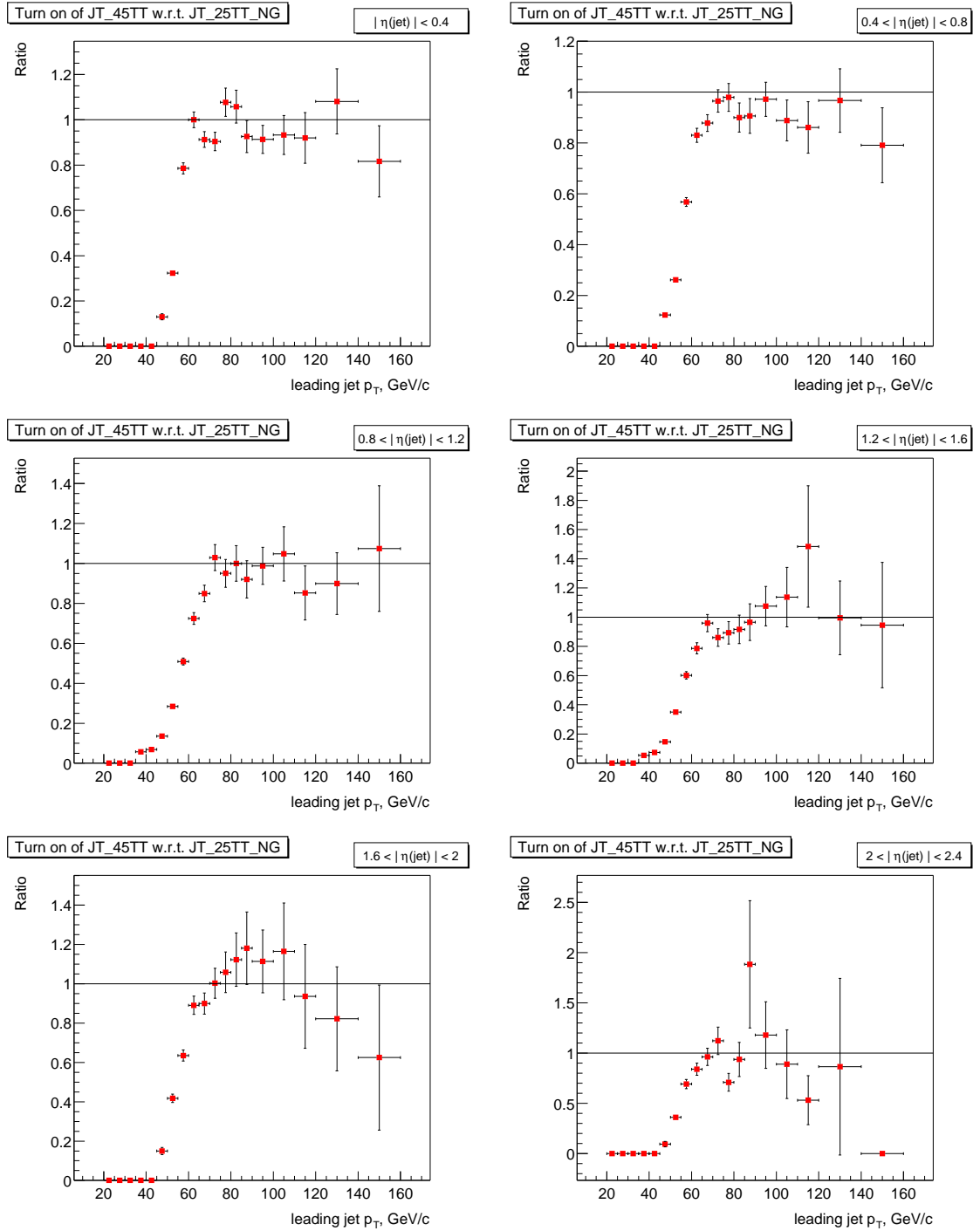


Figure 13: Turn on curves in the different η_{det} bins for JT_45TT trigger with respect to the JT_25TT_NG trigger. For trigger lists v9.31 — v9.50.

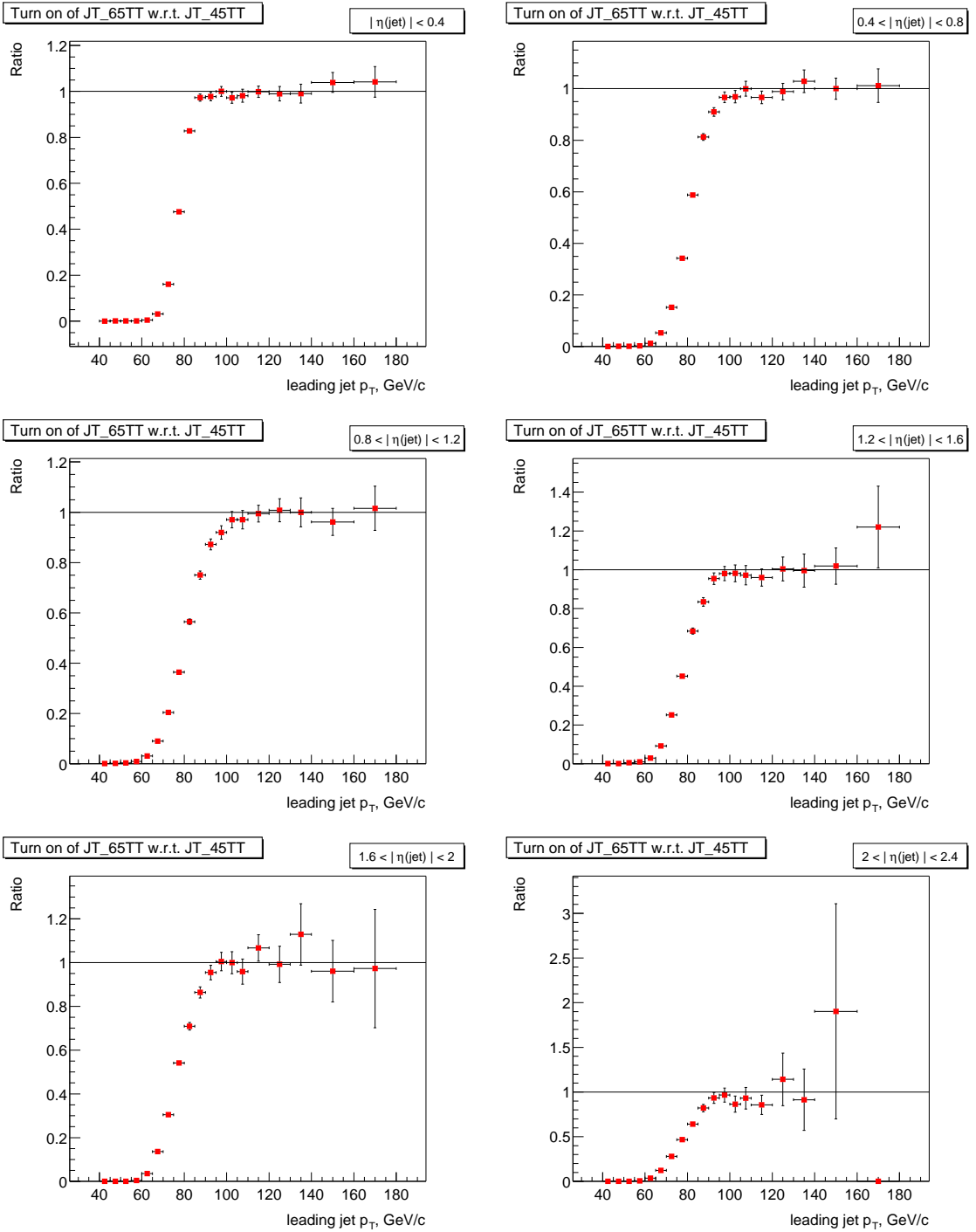


Figure 14: Turn on curves in the different η_{det} bins for JT_65TT trigger with respect to the JT_45TT trigger. For trigger lists v9.31 — v9.50.

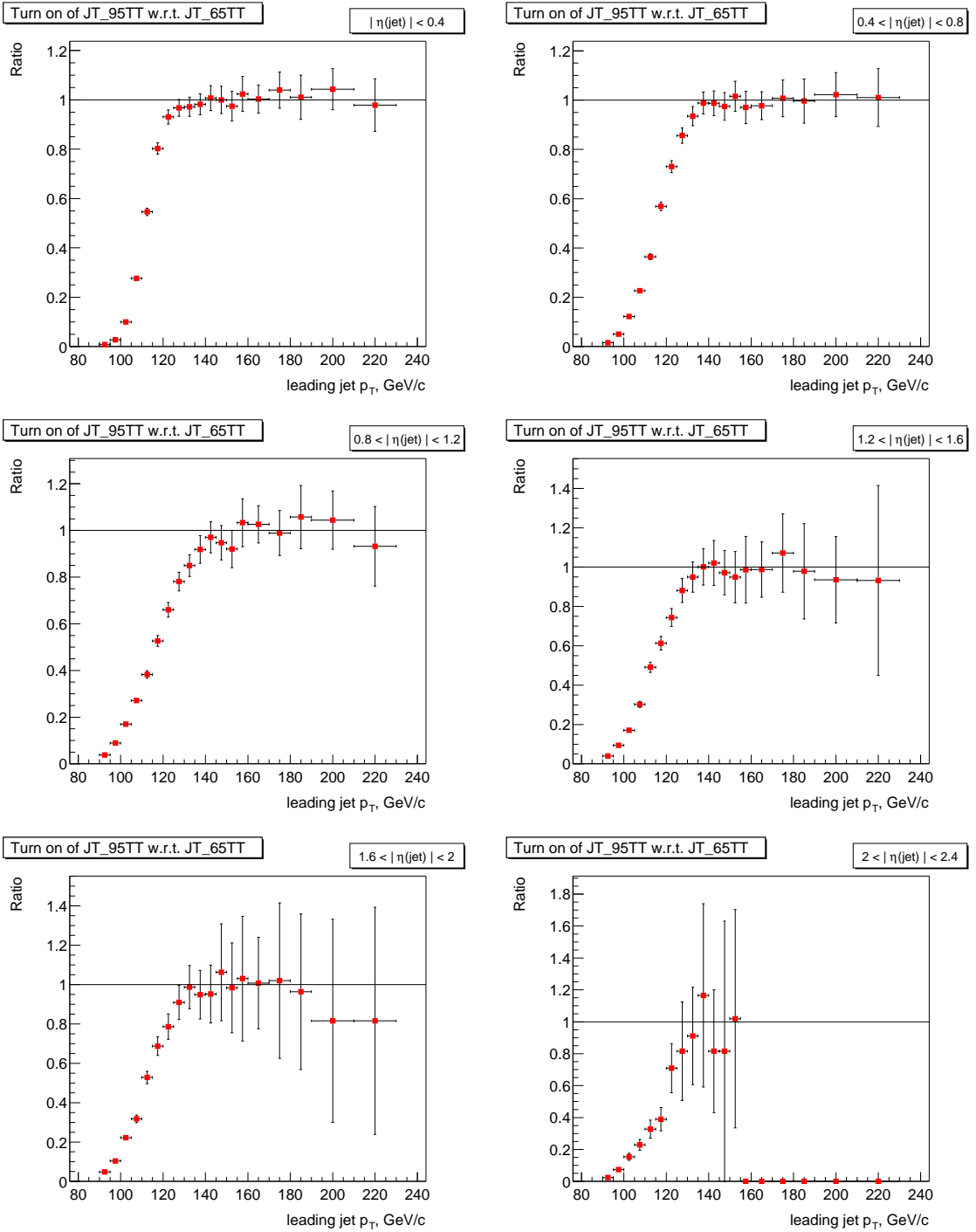


Figure 15: Turn on curves in the different η_{det} bins for JT_95TT trigger with respect to the JT_65TT trigger. For trigger lists v9.31 — v9.50.

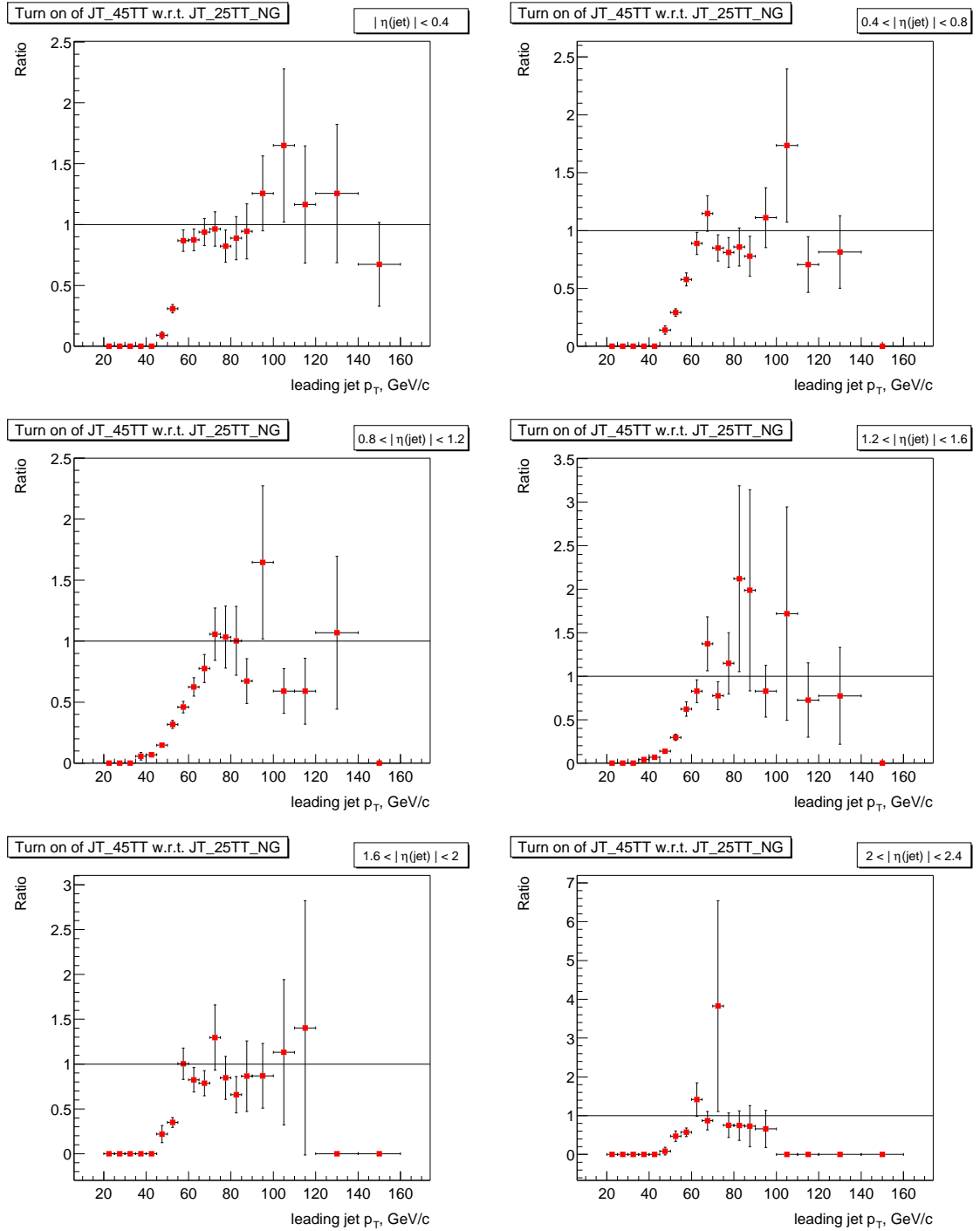


Figure 16: Turn on curves in the different η_{det} bins for JT_45TT trigger with respect to the JT_25TT_NG trigger. For trigger lists v10.00, v10.03 — v10.36.

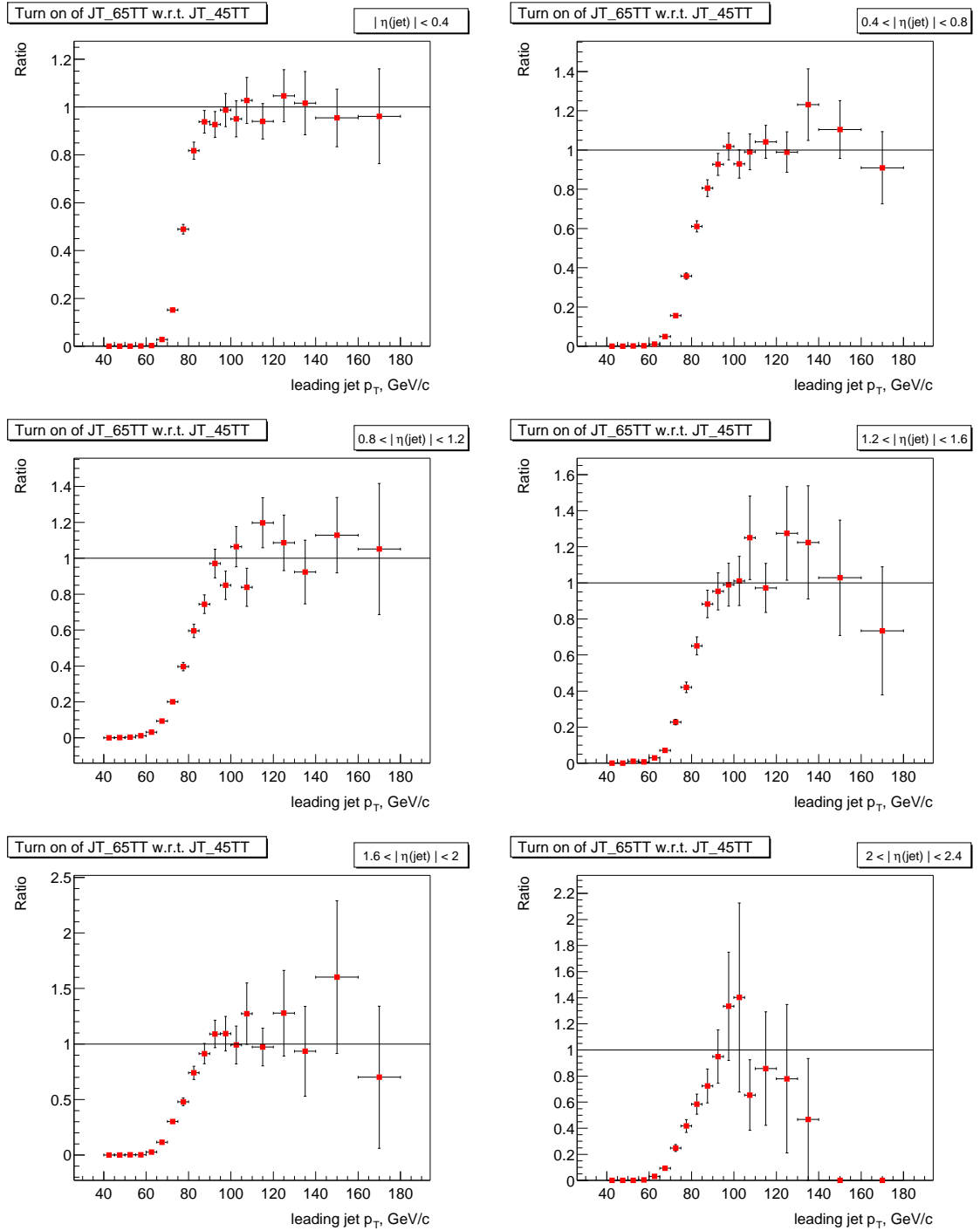


Figure 17: Turn on curves in the different η_{det} bins for JT_65TT trigger with respect to the JT_45TT trigger. For trigger lists v10.00, v10.03 — v10.36.

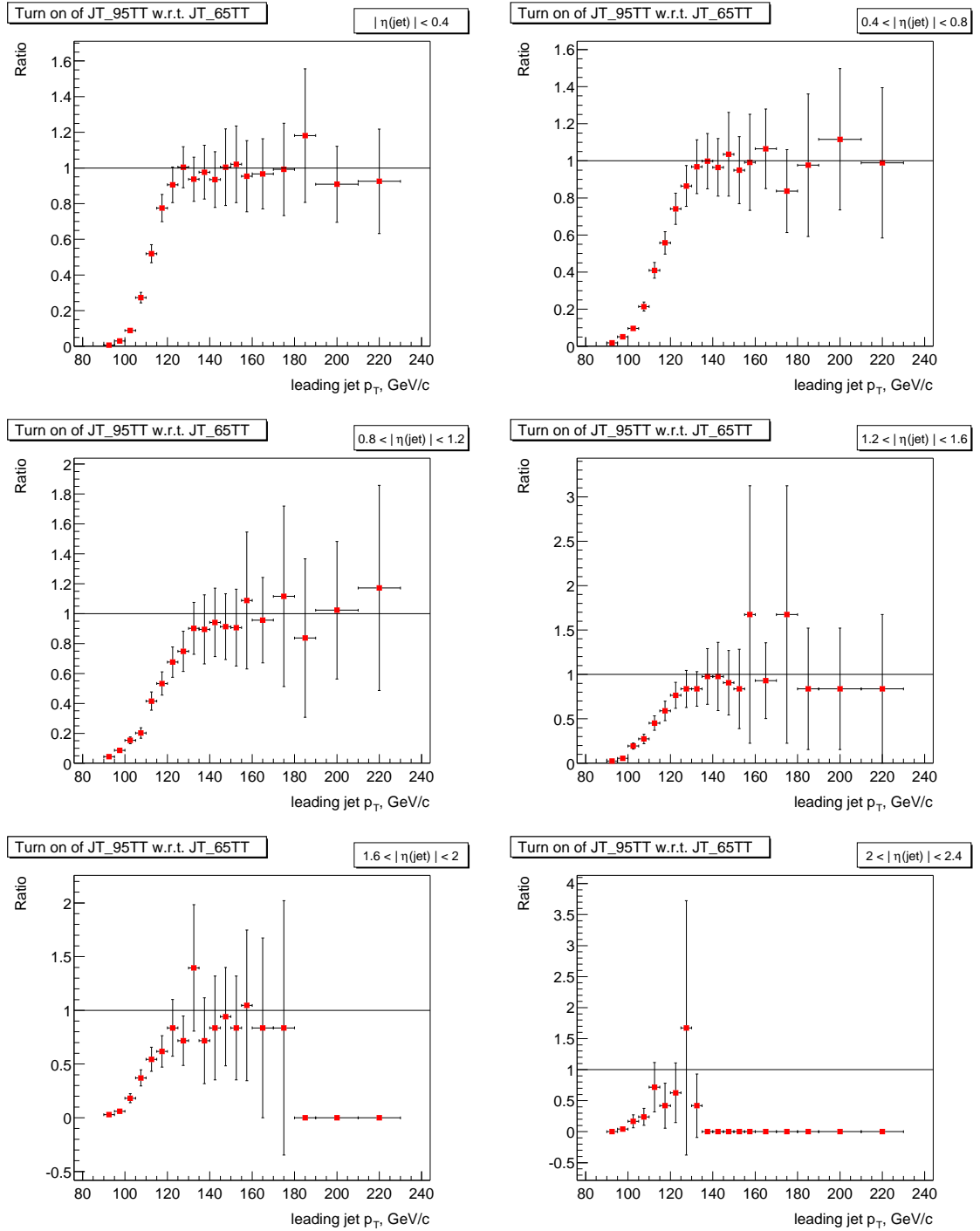


Figure 18: Turn on curves in the different η_{det} bins for JT_95TT trigger with respect to the JT_65TT trigger. For trigger lists v10.00, v10.03 — v10.36.

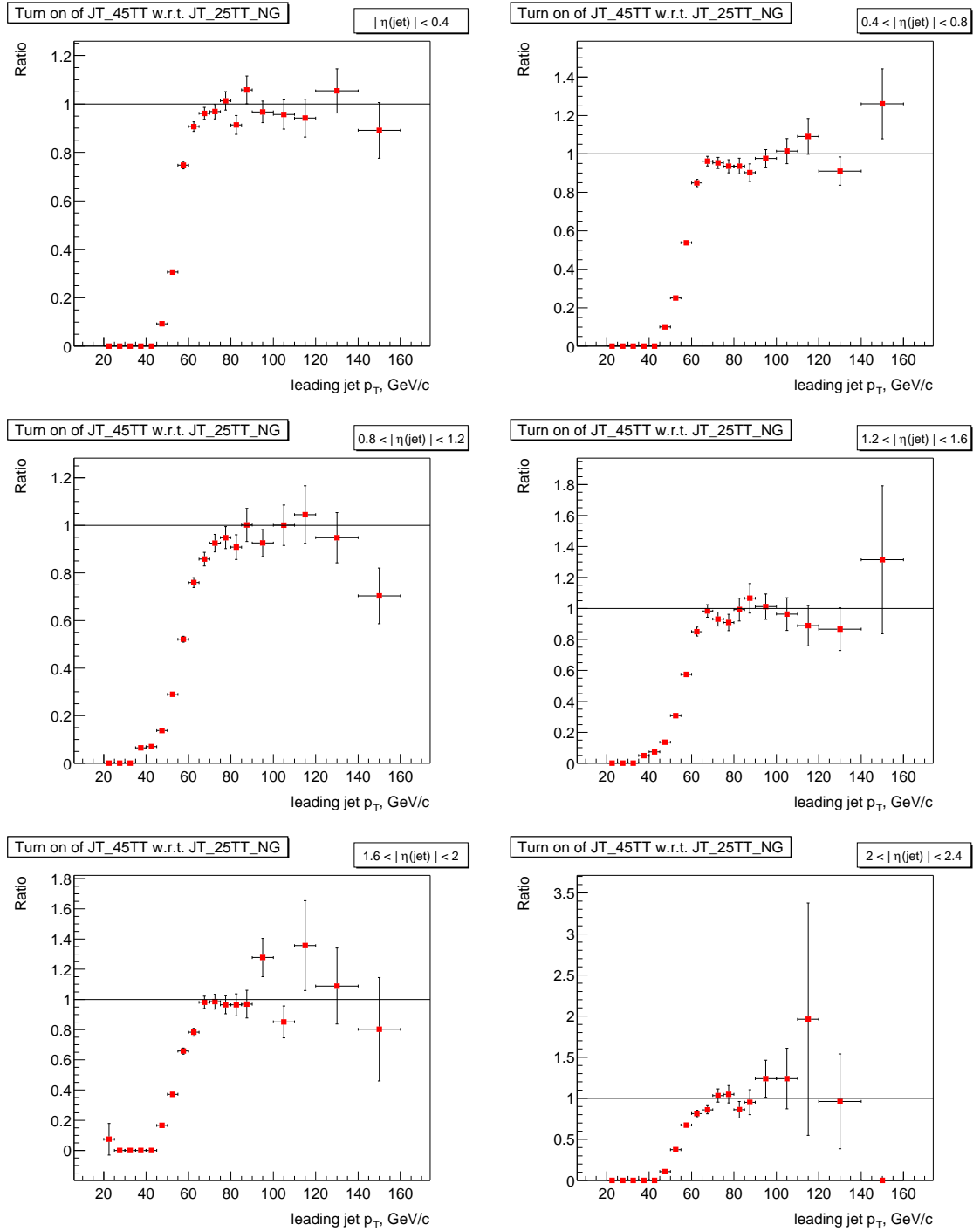


Figure 19: Turn on curves in the different η_{det} bins for JT_45TT trigger with respect to the JT_25TT_NG trigger. For trigger lists v11.00 — v11.04.

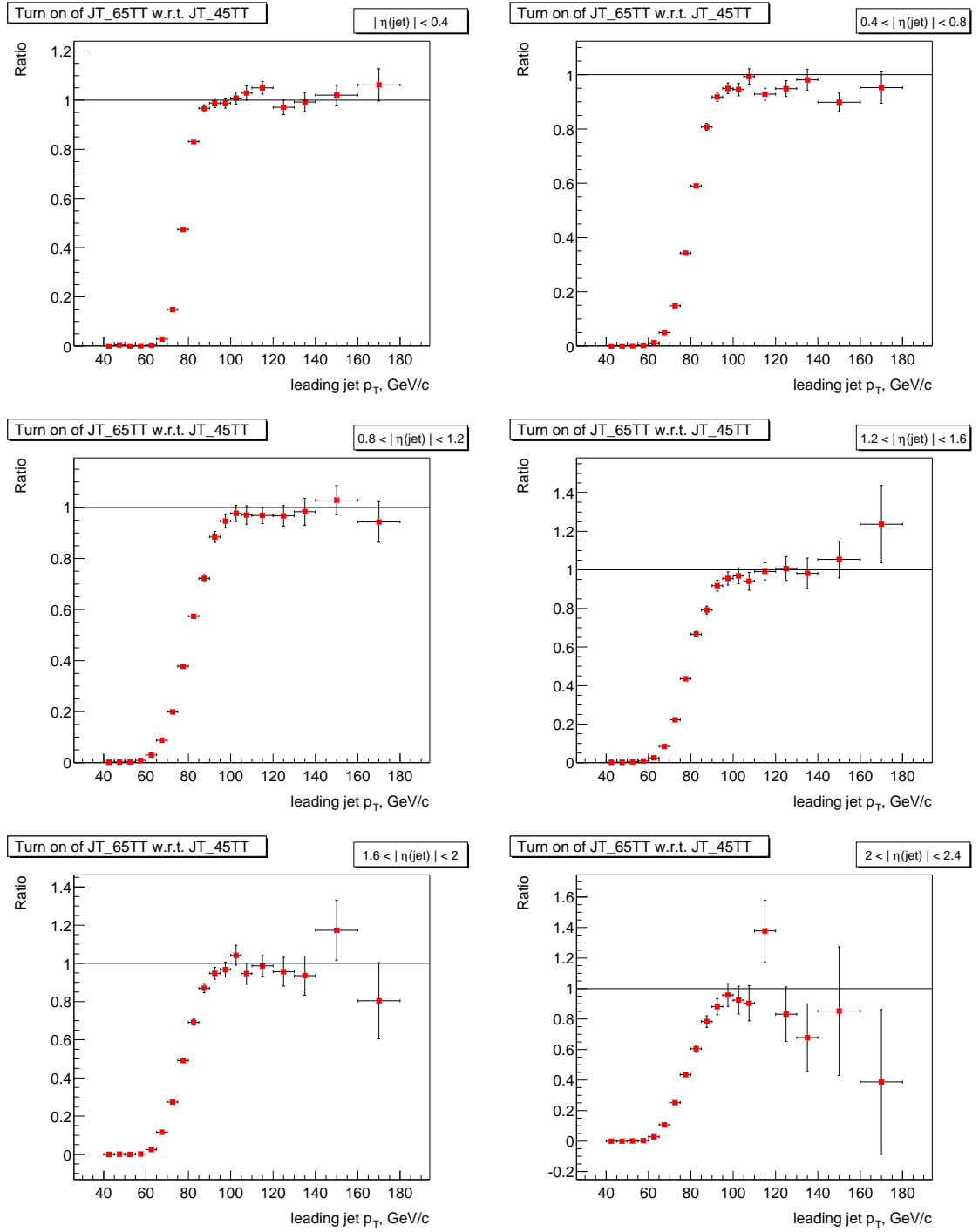


Figure 20: Turn on curves in the different η_{det} bins for JT_65TT trigger with respect to the JT_45TT trigger. For trigger lists v11.00 — v11.04.

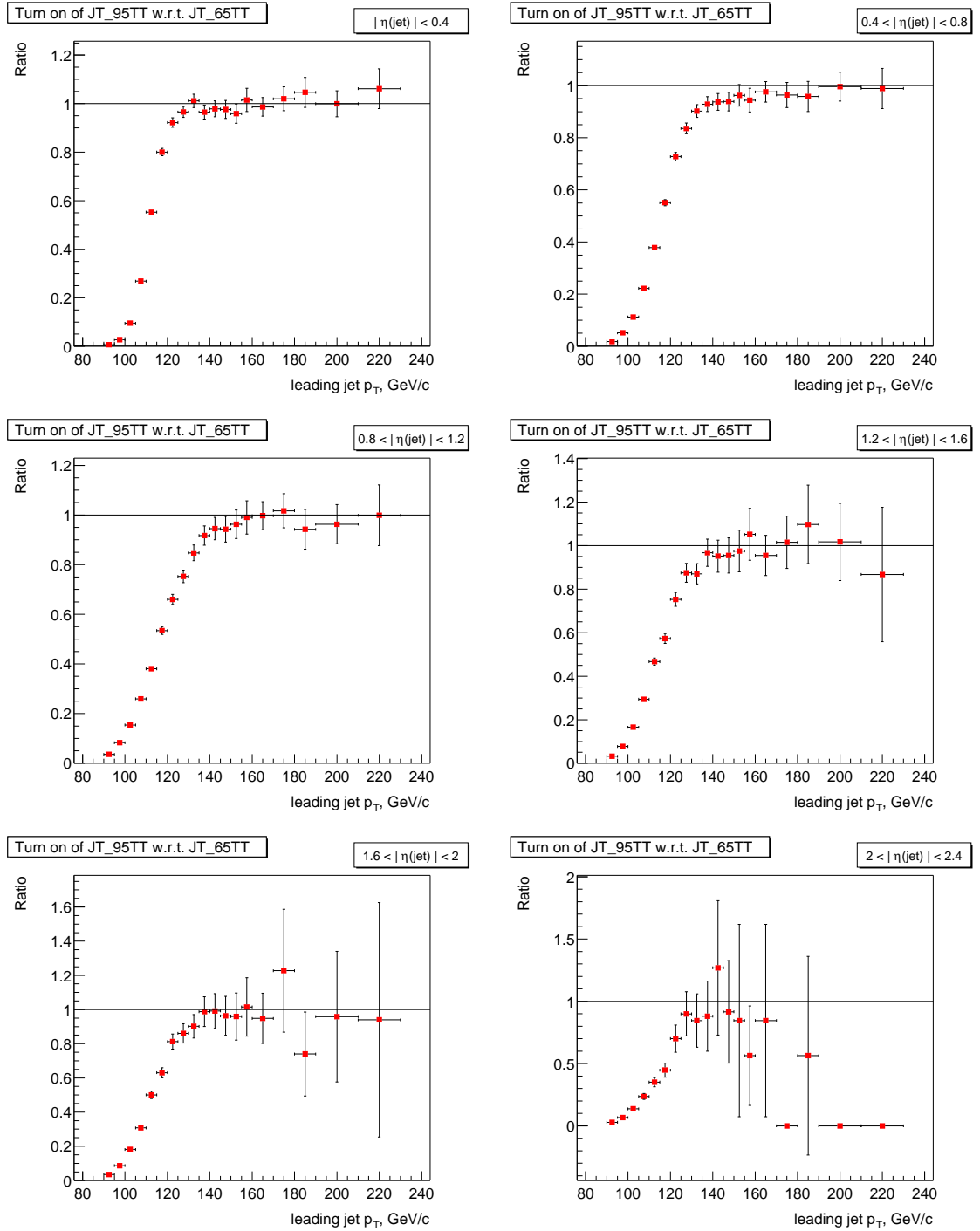


Figure 21: Turn on curves in the different η_{det} bins for JT_95TT trigger with respect to the JT_65TT trigger. For trigger lists v11.00 — v11.04.

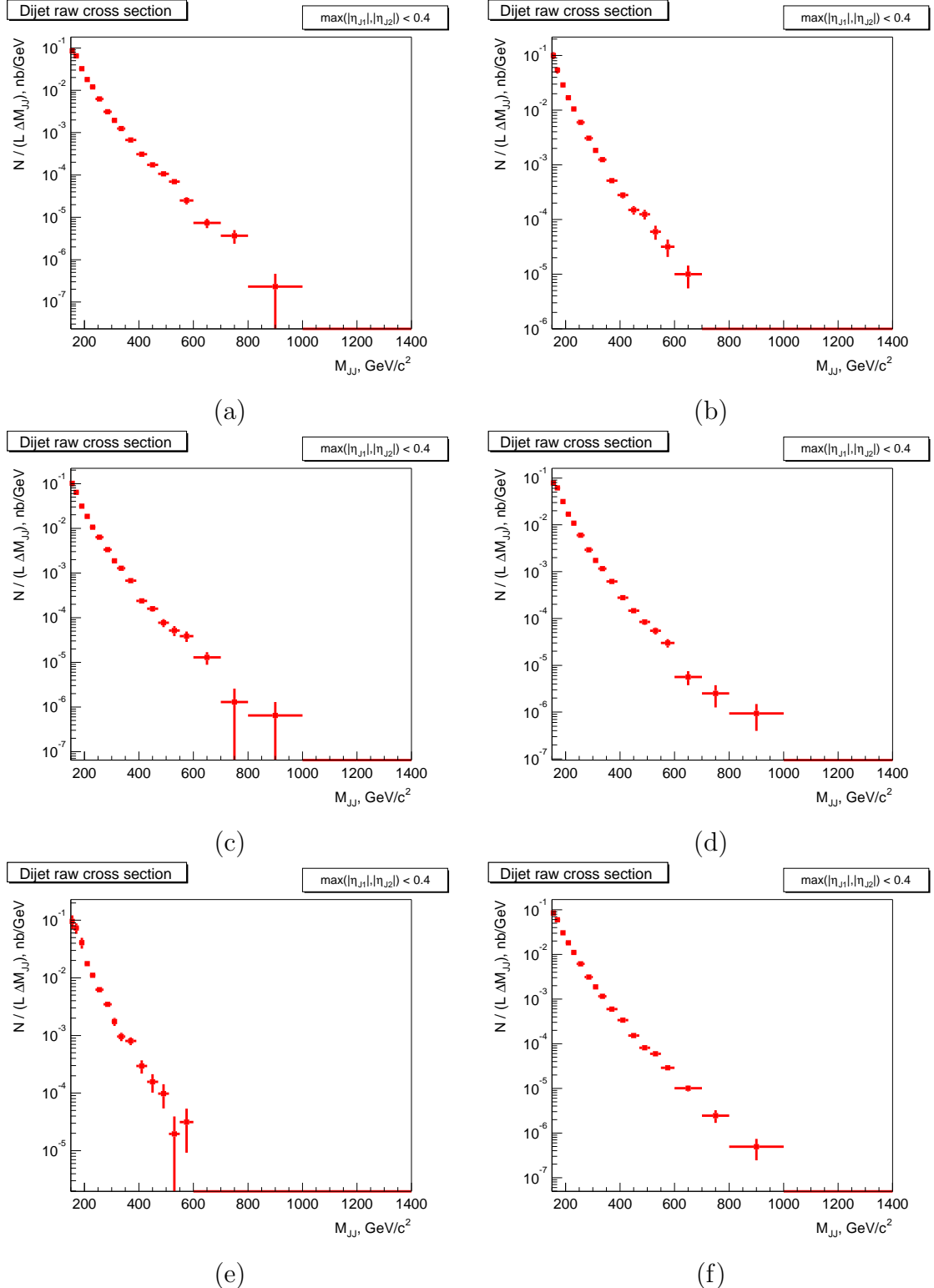


Figure 22: Uncorrected dijet cross sections for $\eta_{max} < 0.4$. For different trigger list versions: v8.20 — v8.41 (a); v9.20 (b); v9.30 (c); v9.31 — v9.50 (d); v10.00, v10.03 — v10.36 (e); v11.00 — v11.04 (f).

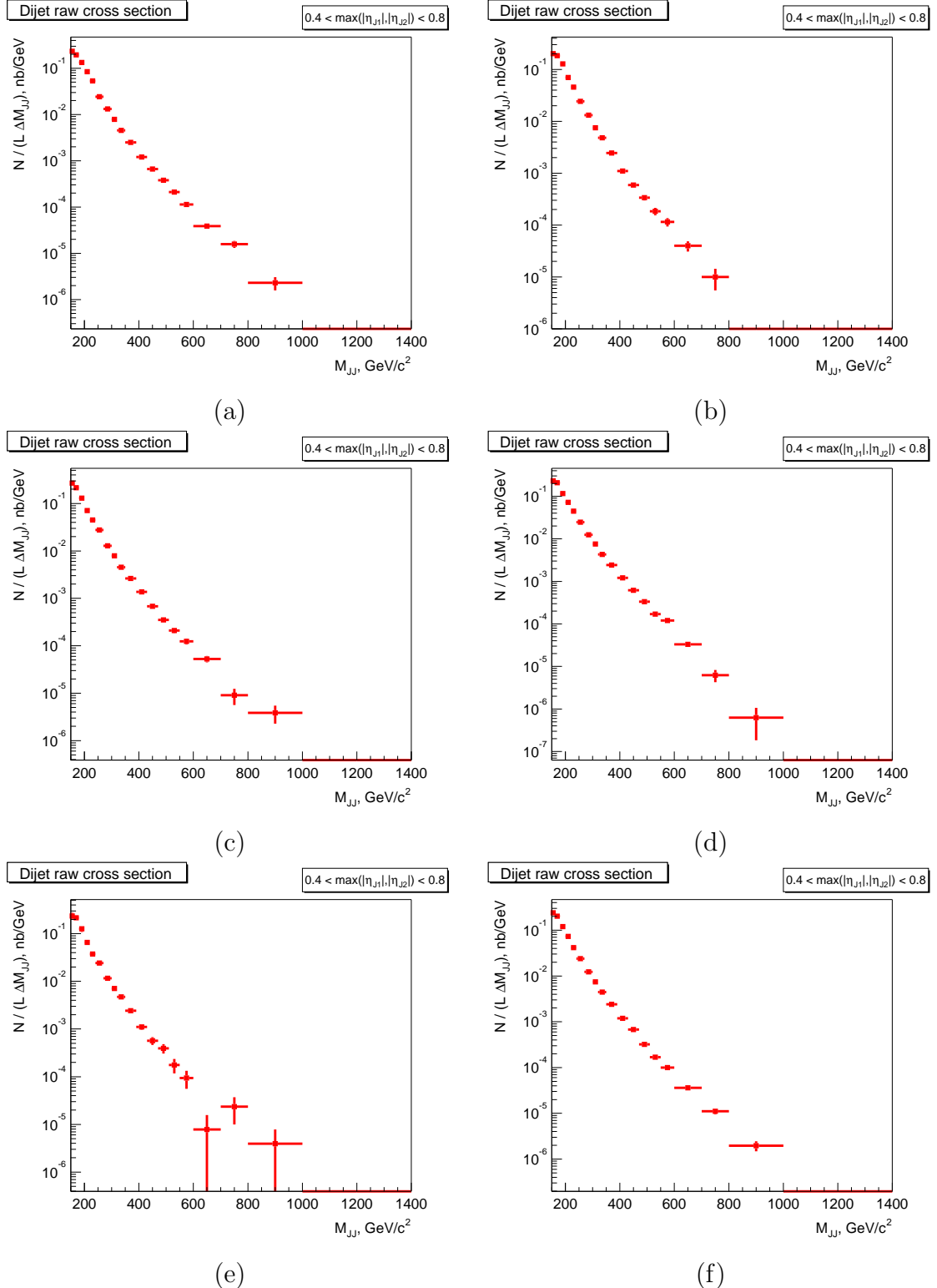


Figure 23: Uncorrected dijet cross sections for $0.4 < \eta_{max} < 0.8$. For different trigger list versions: v8.20 — v8.41 (a); v9.20 (b); v9.30 (c); v9.31 — v9.50 (d); v10.00, v10.03 — v10.36 (e); v11.00 — v11.04 (f).

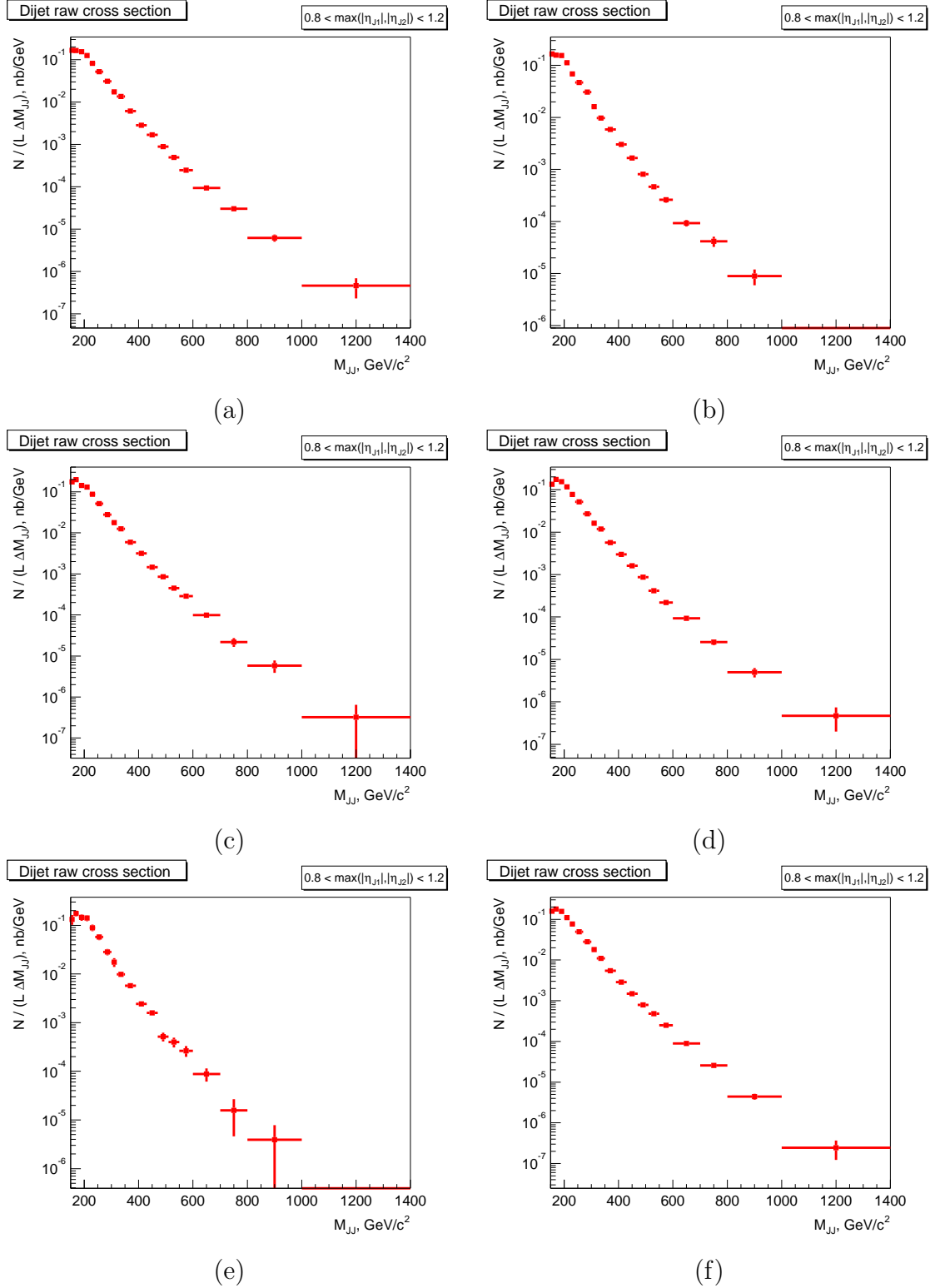


Figure 24: Uncorrected dijet cross sections for $0.8 < \eta_{max} < 1.2$. For different trigger list versions: v8.20 — v8.41 (a); v9.20 (b); v9.30 (c); v9.31 — v9.50 (d); v10.00, v10.03 — v10.36 (e); v11.00 — v11.04 (f).

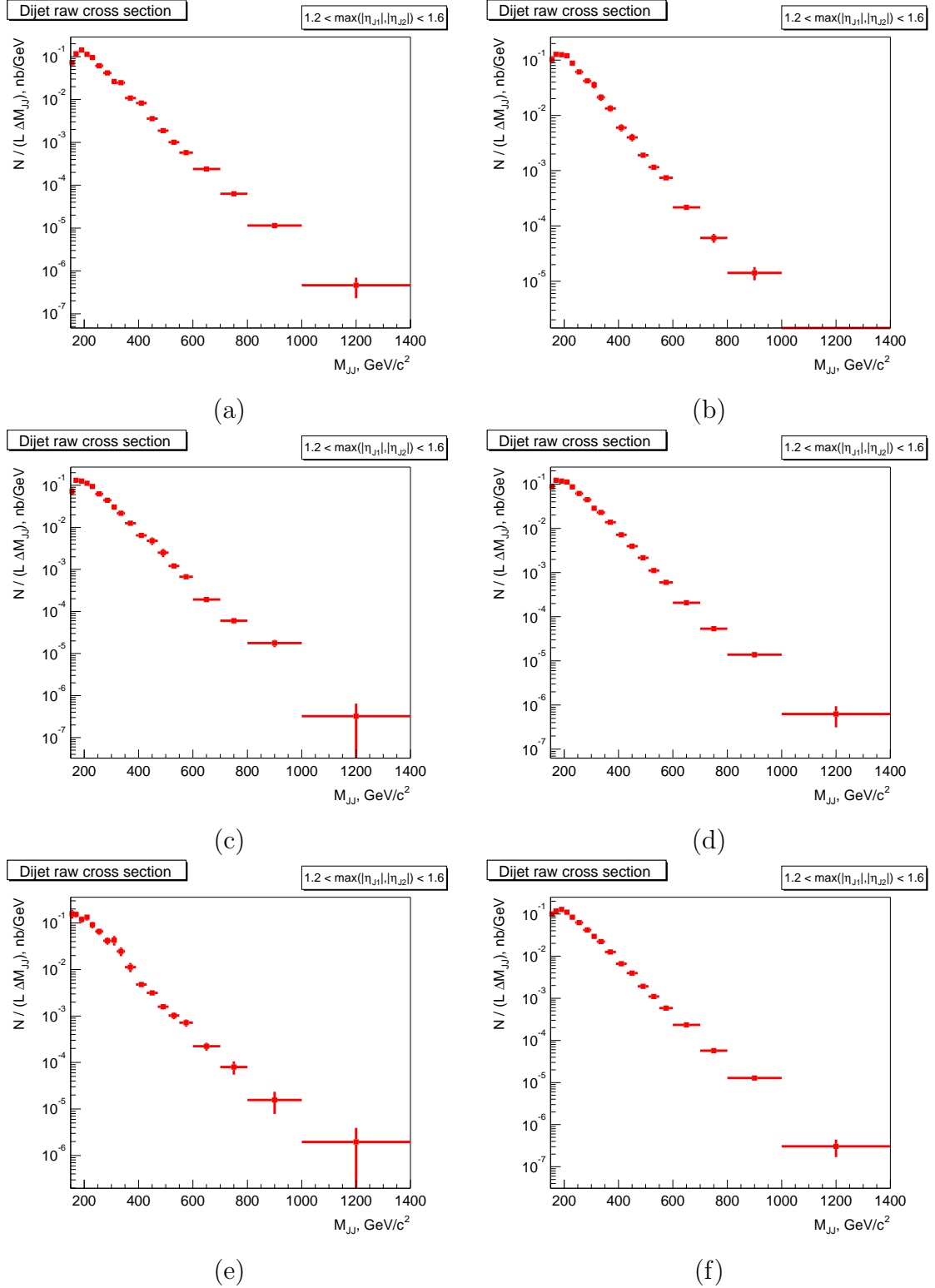


Figure 25: Uncorrected dijet cross sections for $1.2 < \eta_{max} < 1.6$. For different trigger list versions: v8.20 — v8.41 (a); v9.20 (b); v9.30 (c); v9.31 — v9.50 (d); v10.00, v10.03 — v10.36 (e); v11.00 — v11.04 (f).

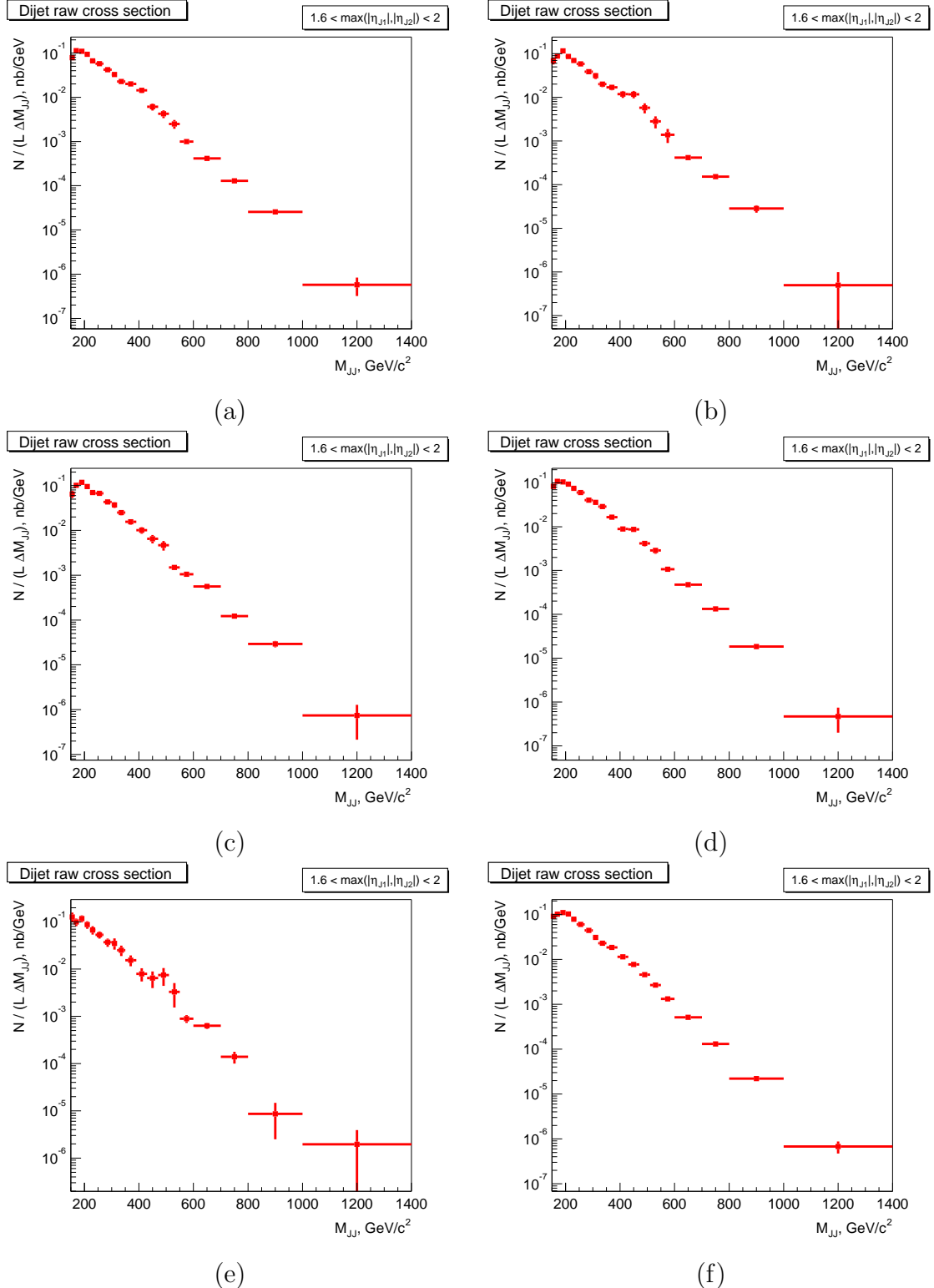


Figure 26: Uncorrected dijet cross sections for $1.6 < \eta_{max} < 2.0$. For different trigger list versions: v8.20 — v8.41 (a); v9.20 (b); v9.30 (c); v9.31 — v9.50 (d); v10.00, v10.03 — v10.36 (e); v11.00 — v11.04 (f).

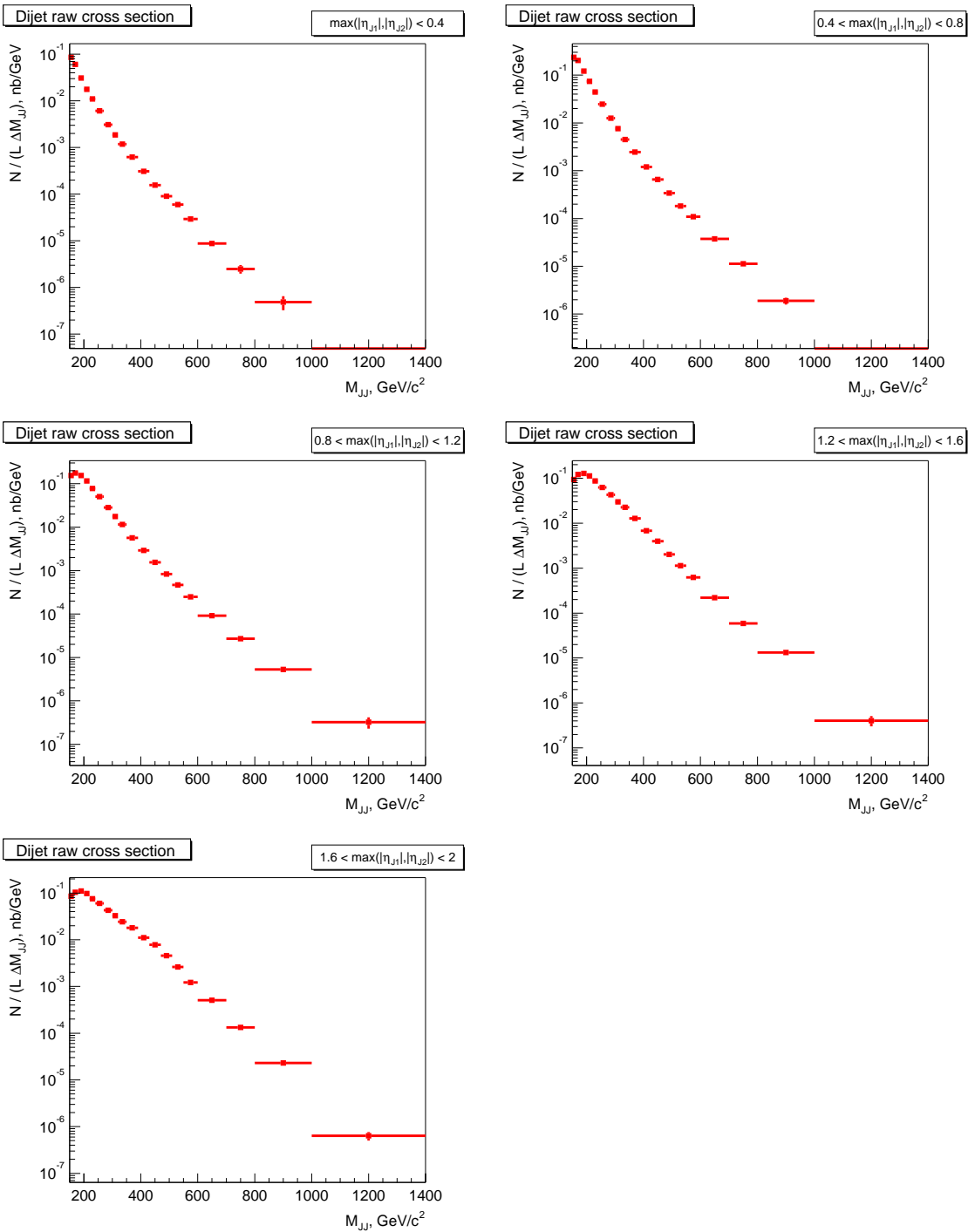


Figure 27: Uncorrected dijet cross sections in the different η_{max} bins. For all trigger list versions.